Contemporary Mathematics
https://ojs.wiserpub.com/index.php/CM/

Research Article

Modeling Dengue-COVID-19 Co-Epidemics via Crossover Discrete Time Systems with Variable-Order Fractional Memory

Seham M. Al-Mekhlafi[1,2*], Ahmed Boudaoui[3], Noura Laksaci[3], Thabet Abdeljawad[4,5,6], Bahaaeldin Abdalla[5]

[1] Department of Mathematics, Faculty of Education, Sana'a University, Sana'a, Yemen
[2] Department of Engineering Mathematics and Physics, Future University in Egypt, Cairo, Egypt
[3] Mathematics Modeling and Applications Laboratory, University of Adrar, Adrar, Algeria
[4] Department of Fundamental Sciences, Faculty of Engineering and Architecture, Istanbul Gelisim University, Avcılar, Istanbul 34310, Turkey
[5] Department of Mathematics and Sciences, Prince Sultan University, P.O. Box 66833, 11586 Riyadh, Saudi Arabia
[6] Department of Mathematics and Applied Mathematics, Sefako Makgatho Health Sciences University, Garankuwa, Medusa 0204, South Africa
E-mail: sih.almikhlafi@su.edu.ye

Received: 20 October 2025; **Revised:** 22 Novembe 2025; **Accepted:** 16 December 2025

Abstract: This paper develops a comprehensive discrete-time mathematical framework to investigate the co-circulation dynamics of two dengue virus strains and COVID-19 by integrating integer-order modeling with advanced fractional and variable-order operators. We formulate four epidemiological models: a classical integer-order system, a fractional Caputo model with constant memory, and two novel crossover models in which the system transitions between fixed- and variable-order fractional operators to represent regime shifts in immunity, behavioral changes, and intervention strategies. This formulation captures nonlocal memory effects and provides a flexible mechanism to describe evolving epidemic phases. A rigorous analytical study is conducted, establishing positivity and boundedness of solutions and proving existence and uniqueness using Perov's fixed-point theorem in a generalized Banach space. The basic reproduction number is derived via the next-generation matrix approach, and local stability of the disease-free equilibrium is characterized. Furthermore, we show that the proposed systems undergo a forward (supercritical) transcritical bifurcation as the basic reproduction number crosses unity. The developed fractional and variable-order models are also shown to satisfy Ulam-Hyers and Lyapunov stability properties. Extensive numerical simulations validate the theoretical findings and demonstrate the role of fractional memory, variable-order dynamics, and crossover transitions in shaping co-epidemic trajectories. The results highlight the importance of incorporating time-varying memory effects in modeling real-world dengue-COVID-19 interactions and provide a robust mathematical framework to support public health planning during co-epidemic scenarios.

Keywords: double strains of COVID-19 and dengue model, crossover discrete systems, variable-order difference operator, numerical simulations

MSC: 92D30, 39A12, 26A33

Copyright ©2026 Seham M. Al-Mekhlafi, et al.
DOI: https://doi.org/10.37256/cm.7420268949
This is an open-access article distributed under a CC BY license
(Creative Commons Attribution 4.0 International License)
https://creativecommons.org/licenses/by/4.0/

1. Introduction

Dengue fever, a re-emerging arboviral infection caused by the Dengue Virus (DENV) of the *Flaviviridae* family, has become a major global health concern. Transmitted primarily by *Aedes aegypti* mosquitoes, dengue manifests as an acute febrile illness characterized by high fever, rash, joint pain, and gastrointestinal disturbances. The virus comprises four antigenically distinct serotypes (DENV-1 to DENV-4), and infection with one serotype provides neither cross-protection nor durable immunity against others. Consequently, secondary infections are associated with an increased risk of severe complications such as dengue hemorrhagic fever and dengue shock syndrome. According to the World Health Organization (WHO), approximately 390 million dengue infections occur annually, with 96 million presenting clinically and a disproportionate burden over 70% falling on Asia [1–5].

Simultaneously, the ongoing COVID-19 pandemic, caused by the Severe Acute Respiratory Syndrome Coronavirus 2 (SARS-CoV-2), has claimed millions of lives and strained health systems worldwide. With over 514 million confirmed infections and more than six million deaths reported globally, COVID-19's clinical presentation spans from asymptomatic and mild symptoms to acute respiratory distress. Its transmission dynamics have evolved through multiple variants (Alpha, Delta, Omicron), each with differing infectiousness and pathogenicity. Although stringent public health interventions such as lockdowns, mask mandates, social distancing, and mass vaccination campaigns have mitigated spread [6, 7], the socioeconomic costs have been profound [8, 9]. Furthermore, the dynamics have evolved through multiple variants [10], and mathematical modeling has been crucial in understanding these complexities [11, 12].

Recent epidemiological evidence has revealed the co-circulation and co-infection of dengue and COVID-19 in several regions. This dual-pathogen scenario exacerbates diagnostic ambiguity due to overlapping symptoms and heightens clinical risks, particularly in areas with weak healthcare infrastructure. Coinfection has been associated with increased hospitalization rates and mortality, further complicating surveillance and control strategies [13–15]. These developments demand advanced mathematical tools to capture the intertwined transmission dynamics, inform public health decisions, and evaluate control strategies in the face of multifaceted epidemics.

Mathematical modeling has long been instrumental in understanding infectious disease dynamics. In particular, Fractional Differential Equations (FDEs) and their discrete analogs have attracted increasing attention due to their capacity to capture memory-dependent processes and nonlocal temporal effects features critical in modeling incubation delays, immune responses, and intervention lags [16–20]. The Caputo-type fractional difference operator is particularly well-suited for epidemiological modeling, as it maintains compatibility with classical initial conditions while enabling the incorporation of memory effects.

The recent advances in variable-order fractional calculus have greatly expanded the modeling capabilities of dynamical systems, particularly in epidemiology and biological processes. The works in [21–28] provide a rigorous mathematical and numerical foundation for variable-order operators, showing how the memory index can evolve with time to represent systems whose dynamics change across different phases. Specifically, the authors in [21] introduce the formal definition and analytical properties of variable-order derivatives, emphasizing their ability to describe non-stationary memory kernels that better match biological and environmental variability. In [22], these ideas are extended to discrete-time settings, where the authors develop practical numerical formulations and demonstrate their improved accuracy compared with classical constant-order models.

Furthermore, the studies in [24, 25] apply variable-order operators to a range of biological and epidemiological models, illustrating that varying the fractional order captures key real-world phenomena such as changing contact behavior, waning immunity, and transitions between epidemic phases. These works show that variable-order approaches often outperform traditional integer-order or fixed fractional-order models when validated against real data. The contributions of [25] include a comprehensive stability analysis framework tailored for variable-order systems, facilitating the study of equilibria, bifurcations, and long-term dynamics in non-stationary environments. Finally, reference [26] develops the discrete-time Caputo type variable-order difference operator employed in the present study, and establishes its core properties, numerical implementation, and convergence behavior.

Collectively, these references provide the theoretical justification and mathematical motivation for employing variable-order fractional discrete systems in the proposed dengue-COVID-19 co-epidemic model. They demonstrate that variable-

order memory is a powerful tool for capturing evolving epidemiological characteristics, thereby yielding more realistic and flexible epidemic dynamics.

Despite these developments, there remains a notable gap in the literature concerning discrete-time co-infection models that jointly incorporate vaccination strategies, memory effects, and variable-order operators. Some recent works have proposed SEIR-based models with feedback control or multi-stage vaccination [29–31], yet few address the layered complexity of co-circulating pathogens in a memory-aware framework.

A pivotal aspect of this study is the adoption of fractional-order operators, specifically the Caputo-type difference operator and its variable-order extension. This choice is fundamentally motivated by the need to incorporate memory effects and non-local dynamics into the epidemic model. Unlike classical integer-order models, fractional calculus accounts for the system's history, making it exceptionally suitable for biological processes where past states such as cumulative exposure, waning immunity, or delayed intervention impacts critically influence future outcomes. The Caputo formulation is selected for its compatibility with standard initial conditions, a necessity for modeling real-world epidemiological data. Furthermore, the extension to variable-order operators allows the model to adaptively capture temporal shifts in population behavior, pathogen transmissibility, and control strategy effectiveness. This modeling framework provides a more nuanced and biologically realistic representation of the co-circulation dynamics than traditional approaches.

The main objective of this study is to develop and analyze novel discrete time epidemiological models that capture the co-circulation dynamics of two dengue virus strains and COVID-19 by incorporating fractional order and variable-order memory effects through Caputo type difference operators. In particular, the work introduces two innovative crossover models that allow the memory characteristics of the system to transition across time intervals reflecting changes in population behavior, immunity, and intervention strategies. The study aims to rigorously investigate the positivity, boundedness, and existence of solutions, derive the basic reproduction number R_0, and perform local stability and bifurcation analyses including the characterization of a forward (supercritical) transcritical bifurcation so as to improve understanding of long-term trends and the governance of co-infection dynamics through control in practical epidemic contexts. We further show that the fractional and variable-order systems satisfy Ulam-Hyers and Lyapunov stability properties.

The rest of this manuscript is organized as follows. Section 2 outlines the essential mathematical preliminaries, including definitions and key properties of the Caputo fractional difference operator and its variable-order extension, which form the foundation for the proposed models. Section 3 introduces three discrete-time epidemiological models to describe the concurrent spread of two dengue strains and COVID-19: an integer-order model, a fractional Caputo operator model Caputo operator, and two novel crossover models that transition between fixed and variable memory regimes. Section 4 presents the analytical framework, investigates the qualitative behavior of the system, including rigorous proofs of positivity and boundedness of solutions and the basic reproduction number R_0 is derived via the next-generation matrix method, and local stability conditions for the disease-free equilibrium are established. Also, assess the sensitivity of key epidemiological parameters. Section 5 establishes the existence and uniqueness of solutions for the variable-order system using Perov's fixed-point Theorem in a generalized Banach space and we perform a thorough stability analysis of the proposed fractional-order co-circulation model, demonstrating its Ulam-Hyers and Lyapunov stability properties. In section 6, we formulate the two crossover models that incorporate dynamic transitions between Caputo and variable-order operators to reflect real-world shifts in immunity and intervention strategies. Finally, section 7 presents comprehensive numerical simulations to validate the theoretical results, highlight the role of fractional memory and crossover effects as well as a detailed bifurcation analysis that confirms the presence of a forward (supercritical) transcritical bifurcation. Lastly, section 8 concludes the paper, summarizing major takeaways, their relevance in policymaking, and outlining avenues for further research and work.

2. Notations and preliminaries

We review some key definitions of fractional calculus in this section, which are used in the subsequent portions of the study. We consider that all functions are defined on set $\mathbb{N}_a := \{a,\ a+1,\ a+2,\ ...\}$, where $a \in \mathbb{R}$.

Definition 1 The ζ^{th}-fractional sum of the function $\vartheta : \mathbb{N}_a \longrightarrow \mathbb{R}$ is defined by [19, 32]:

$$\triangle_a^{-\zeta}\vartheta(t)=\frac{1}{\Gamma(\zeta)}\sum_{\tau=a}^{t-\zeta}(t-\tau-1)^{\zeta-1}\vartheta(\tau), \tag{1}$$

for $t\in\mathbb{N}_{a+\zeta}$, $\zeta>0$, $\Gamma(.)$ represents the Euler gamma function and

$$t^{(\zeta)}=\frac{\Gamma(1+t)}{\Gamma(1-\zeta+t)}.$$

Definition 2 For the function $\vartheta(t)$ defined on $\mathbb{N}_a$, the ζ^{th}-order Riemann-Liouville fractional difference operator is formulated in [32].

$$\triangle_a^{\zeta}\vartheta(t):=\triangle\triangle_a^{-(1-\zeta)}\vartheta(t)$$

$$=\frac{1}{\Gamma(\zeta)}\triangle\sum_{\tau=a}^{t-(1-\zeta)}(t-\tau-1)^{-\zeta}\vartheta(\tau), \tag{2}$$

for $t\in\mathbb{N}_{a-\zeta+1}$, $1>\zeta>0$.

Definition 3 The function defined on $\mathbb{N}_a$ has a ζ^{th}-order Caputo fractional difference operator, as described by [32]

$$\begin{cases} {}^{C}\triangle_a^{\zeta}\vartheta(t)=\triangle_a^{-(1-\zeta)}\triangle\vartheta(t)=\dfrac{1}{\Gamma(\zeta)}\displaystyle\sum_{\tau=a}^{t-(1-\zeta)}(t-\tau-1)^{-\zeta}\triangle\vartheta(\tau), & 1>\zeta>0,\\ \triangle\vartheta(t),\ \zeta=1, \quad t\in\mathbb{N}_{a-\zeta+1}. \end{cases}$$

Proposition 1 Let $\vartheta(t)$ be a function defined on $\mathbb{N}_a$. Then [32]

$$\triangle_{a+(1-\zeta)}^{-\zeta}{}^{C}\triangle^{\zeta}\vartheta(t)=\vartheta(t)-\vartheta(a),\ \forall t\in\mathbb{N}_a,\ 1\geq\zeta>0. \tag{3}$$

Proposition 2 Consider $\vartheta(t)$ a function defined in $\mathbb{N}_a$. Then [32]

$${}^{C}\triangle^{\zeta}\vartheta(t)=\triangle_a^{\zeta}\vartheta(t)-\frac{(t-a)^{-\zeta}}{\Gamma(1-\zeta)}\vartheta(a), \quad \forall t\in\mathbb{N}_{a-\zeta+1},\ 1\geq\zeta>0. \tag{4}$$

Lemma 1 Assume $\zeta>0$, $\zeta\notin\mathbb{N}$, and $\vartheta(t)$ be a function defined on $\mathbb{N}$. Then [32]

$$\vartheta(t)=\vartheta(a)+\frac{1}{\Gamma(\zeta)}\sum_{\tau=a+1-\zeta}^{t-\zeta}(t-\tau-1)^{\zeta-1}{}^{C}\triangle^{\zeta}{}_{a}\vartheta(\tau), \quad \forall\rho\in\mathbb{N}_{a+1}. \tag{5}$$

Theorem 1 Consider the following fractional-order difference equations [33]

$$
\begin{aligned}
&{}^{C}\triangle_{a}^{\zeta}\vartheta(t)=\Upsilon(t+\zeta-1,\ \vartheta(t+\zeta-1)),\\
&\vartheta(a)=u_{\kappa},\\
&m=\lceil\zeta\rceil+1,\quad \kappa=0,\ 1,\ ...,\ m-1.
\end{aligned}
\tag{6}
$$

Following that, the discrete integral equation (6) that corresponds to both equations is

$$
\vartheta(t)=\vartheta_{0}(t)+\frac{1}{\Gamma(\zeta)}\sum_{\tau=a+m-\zeta}^{t-\zeta}(t-\tau-1)^{\zeta-1}\Upsilon(\tau+\zeta-1,\ \vartheta(\tau+\zeta-1)),
\tag{7}
$$

where, $\rho\in\mathbb{N}_{a+m}$,

$$
\vartheta_{0}(t)=\sum_{\kappa=0}^{m-1}(t-a)^{(\kappa)}(\Gamma(\kappa+1))^{-1}\triangle^{\kappa}\vartheta(a).
\tag{8}
$$

2.1 *Justification for the fractional-order framework*

The formulation of our epidemiological models using fractional-order discrete calculus is driven by several critical mathematical and biological considerations:

1. **Memory and Hereditary Properties:** Integer-order difference equations are inherently memoryless. However, the transmission dynamics of infectious diseases are strongly influenced by past events. The fractional-order difference operator ${}^{C}\Delta_{a}^{\zeta}$, with its non-local kernel, intrinsically captures these memory effects. This is essential for modeling phenomena such as:

• **Incubation Periods:** The progression from exposure to infectiousness depends on the history of exposure.

• **Immune Response:** The development, duration, and waning of immunity are processes that unfold over time, dependent on the cumulative history of infection and recovery.

• **Intervention Efficacy:** The impact of public health measures (e.g., lockdowns, vaccination campaigns) is not instantaneous but accumulates and decays over time.

2. **Biological Fidelity and Model Flexibility:** The order of the fractional derivative, $\zeta\in(0,\ 1]$, serves as a tunable parameter that can reflect the sub-diffusive nature of disease spread in complex, heterogeneous environments. A lower value of ζ corresponds to a stronger memory effect and a slower, more anomalous diffusion of the disease, often providing a better fit to real-world data than the exponential decay/growth implied by integer-order models.

3. **The Caputo Operator Advantage:** We specifically employ the Caputo-type fractional difference due to its principal advantage for initial value problems: it requires initial conditions on the function itself (e.g., $S_H(a)$, $I_{D1}(a)$), which are standard, measurable quantities. This contrasts with the Riemann-Liouville definition, which requires initial conditions on fractional integrals, which lack a direct physical interpretation.

4. **Generalization via Variable-Order Calculus:** The extension to a variable-order operator $\zeta(t)$ is a natural progression to model systems with evolving dynamics. This allows the "memory length" of the system to change over time, reflecting real-world transitions such as:

• The emergence of more/less transmissible viral variants.

• Seasonal changes in vector activity for dengue.

• Phased implementation or relaxation of non-pharmaceutical interventions.

• Time-dependent waning of vaccine-induced or natural immunity.

This fractional framework, therefore, provides a more powerful and physiologically structured approach to modeling the complex, temporal interactions inherent in the co-circulation of dengue and COVID-19.

3. Mathematical model

In this section, we provide three discrete-time models for controlling the double strains of COVID-19 and dengue co-circulating with integer order, fractional order, and variable order. These models are presented as follows:

3.1 *Integer-order discrete model*

The total human population, denoted by $N_H(t)$, is categorized into the following mutually exclusive compartments: $R_C(t)$, $I_{D1}(t)$, $I_{D2}(t)$, $S_H(t)$, $I_C(t)$, $I_{DC1}(t)$, $I_{DC2}(t)$, $R_D(t)$. These compartments are defined in Table 1 and satisfy the relation [34]:

$$N_H(t) = I_{D1}(t) + I_{D2}(t) + S_H(t) + I_C(t) + I_{DC1}(t) + I_{DC2}(t) + R_D(t) + R_C(t).$$

Similarly, let $N_V(t)$ represent the total mosquito population, divided into the following compartments: $S_V(t)$, $I_{V1}(t)$, $I_{2V}(t)$, are defined in Table 1, and such that [34]:

$$N_V(t) = I_{1V}(t) + I_{2V}(t) + S_V(t).$$

Table 1. The system's variables [34]

The variable	Description
S_H	Uninfected individuals.
I_{D1}	Individuals infected with strain one of dengue
I_{D2}	Individuals infected with strain two of dengue
I_C	Individuals with coronavirus infection
R_D	People who healed from both strains of dengue
R_C	Recuperation from coronavirus
S_V	Not-infected (vulnerable) carriers
I_{V1}	Vector infected with strain one of dengue
I_{V2}	Vectors contaminated with strain two of dengue
I_{DC1}	Individuals co-infected with both coronavirus and first strain of dengue
I_{DC2}	Individuals co-infected with coronavirus and dengue strain two

Uninfected individuals (S_H) enter the population at a recruitment rate of Λ_H. The population decreases due to natural mortality, as well as infections from dengue strain one, dengue strain two, and coronavirus. The transmission rates for these infections depend on contact with infected vectors or individuals.

- $\lambda_{V1} = \dfrac{\beta_{V1} I_{V1}}{N_H}$, representing transmission from vectors carrying dengue strain one.
- $\lambda_{V2} = \dfrac{\beta_{V2} I_{V2}}{N_H}$, representing transmission from vectors carrying dengue strain two.

• $\lambda_C = \dfrac{\beta_C(I_C + I_{DC1} + I_{DC1})}{N_H}$, representing transmission from humans infected with coronavirus, with β_C being the contact rate.

Recovered individuals may lose immunity to dengue at a rate θ_D, becoming susceptible again. Similarly, individuals who recover from coronavirus lose immunity at a rate θ_C. We assume a consistent natural mortality rate for all individuals, occurring at a rate m_H.

For vectors, susceptibility is reduced due to infection with either dengue strain one or two. The transmission rates for these infections are:

• $\lambda_{D1} = \dfrac{\beta_{D1}(I_{D1} + I_{DC1})}{N_H}$, for dengue strain one.

• $\lambda_{D2} = \dfrac{\beta_{D2}(I_{D2} + I_{DC2})}{N_H}$, for dengue strain two. Vector mortality occurs at a rate m_V.

Table 2 defines other parameters.

Table 2. Parameter values [34]

Parameter	Description	Value
Λ_H	Constant recruiting rate for individuals.	156.1898
β_{D1}	Rate of transmission of Dengue strain 1 from humans to vectors	0.60
β_{D2}	Rate of transmission of Dengue strain 2 from humans to vectors	0.62
β_C	Rate of coronavirus transmission	0.8368
θ_C	Loss of acquired resistance to the coronavirus	0.00000043117
θ_D	Loss of acquired immunity against dengue	0.026
Λ_V	Regular rate of vector recruitment	1500
ε_{v1}	Parameter modification that accounts for coronavirus-infected individuals' vulnerability to dengue strain one	1
ε_{v2}	Parameter modification that accounts for coronavirus-infected individuals' vulnerability to dengue strain two	1
ε_C	Parameter modification that accounts for dengue-infected individuals' vulnerability to the coronavirus	1
τ_{D1}	Recovery rate for dengue strain one	0.17
τ_{D2}	Recovery rate for dengue strain two	0.15
d_{D1}	Death rate from dengue strain one	0.0012
d_{D2}	Death rate from dengue strain two	0.001
β_{V1}	Rate of transmission of Dengue strain 1 from vector to human	0.0100
β_{V2}	Rate of transmission of Dengue strain 2 from vector to human	0.0747
τ_C	rate of coronavirus recovery	0.7031
m_H	People's natural death rate	3.6578e-05
m_V	rate of vector elimination	0.0476

Based on the flowdiagram in Figure 1, the following description of the two strains of dengue and COVID-19 co-circulating epidemic integer order model. This model is developed using the reference [33] as a foundational framework. However, our work introduces several key novelties to capture the complexity of co-circulation more realistically. Specifically, we have incorporated **co-infection compartments** (I_{DC1} and I_{DC2}) to explicitly model individuals simultaneously infected with both COVID-19 and each dengue strain, a feature not present in [33]. Furthermore, we have integrated a more detailed cross-susceptibility mechanism, including parameters (ε_C, ε_{v1}, ε_{v2}) that modulate the infection rates for individuals already infected with one pathogen. These additions are crucial for representing the synergistic dynamics and increased clinical risks observed in real-world co-epidemic scenarios.

$$S_H(t_{\rho+1}) = S_H(t_\rho) + \Lambda_H - \left(\frac{\beta_{V2} I_{V2}(t_\rho)}{N_H(t_\rho)} + \frac{\beta_C(I_{DC2}(t_\rho) + I_{DC1}(t_\rho) + I_C(t_\rho))}{N_H(t_\rho)} + \frac{\beta_{V1} I_{V1}(t_\rho)}{N_H(t_\rho)} \right)$$

$$S_H(t_\rho) - m_H S_H(t_\rho) + \theta_C R_C(t_\rho) + \theta_D R_D(\rho),$$

$$I_{D1}(t_{\rho+1}) = I_{D1}(t_\rho) + \frac{\beta_{V1} I_{V1}(t_\rho)}{N_H(t_\rho)}(S_H(t_\rho) + R_C(t_\rho)) - (\tau_{D1} + d_{D1} + m_H) I_{D1}(t_\rho)$$

$$- \varepsilon_C \frac{\beta_C (I_{DC2}(t_\rho) + I_{DC1}(t_\rho) + I_C(t_\rho))}{N_H(t_\rho)} I_{D1}(t_\rho)$$

$$+ \tau_C I_{DC1}(t_\rho),$$

$$I_{D2}(t_{\rho+1}) = I_{D2}(t_\rho) + \frac{\beta_{V2} I_{V2}(t_\rho)}{N_H(t_\rho)}(S_H(t_\rho) + R_C(t_\rho)) - (\tau_{D2} + d_{D2} + m_H) I_{D2}(t_\rho)$$

$$+ \varepsilon_C \frac{\beta_C (I_{DC2}(t_\rho) + I_{DC1}(t_\rho) + I_C(t_\rho))}{N_H(t_\rho)} I_{D2}(t_\rho)$$

$$+ \tau_C I_{DC2}(t_\rho) + \zeta - 1),$$

$$I_C(t_{\rho+1}) = I_C(t_\rho) + \frac{\beta_C (I_C(t_\rho) + I_{DC1}(t_\rho) + I_{DC2}(t_\rho))}{N_H(t_\rho)}(S_H(t_\rho) + R_D(t_\rho))$$

$$- (\tau_C + d_C + m_H) I_C(t_\rho) + \tau_{D1} I_{DC1}(t_\rho)$$

$$+ \tau_{D2} I_{DC2}(t_\rho) - \left(\varepsilon_{v2} \frac{\beta_{V2} I_{V2}(t_\rho)}{N_H(\rho)} + \varepsilon_{v1} \frac{\beta_{V1} I_{V1}(t_\rho)}{N_H(t_\rho)} \right) I_C(t_\rho),$$

$$I_{DC1}(t_{\rho+1}) = I_{DC1}(t_\rho) + \varepsilon_C \frac{\beta_C (I_{DC2}(t_\rho) + I_{DC1}(t_\rho) + I_C(t_\rho))}{N_H(t_\rho)} I_{D1}(t_\rho)$$

$$+ \varepsilon_{v1} \frac{\beta_{V1} I_{V1}(t_\rho)}{N_H(t_\rho)} I_C(t_\rho) - (\tau_{D1} + d_{D1} + m_H + \tau_C + d_C) I_{D1}(t_\rho),$$

$$I_{DC2}(t_{\rho+1}) = I_{DC2}(t_\rho) + \varepsilon_C \frac{\beta_C (I_{DC2}(t_\rho) + I_{DC1}(t_\rho) + I_C(t_\rho))}{N_H(t_\rho)} I_{D2}(t_\rho)$$

$$+ \varepsilon_{v2} \frac{\beta_{V2} I_{V2}(t_\rho)}{N_H(t_\rho)}) I_C(t_\rho) - (\tau_{D2} + d_{D2} + m_H + \tau_C + d_C) I_{D2}(t_\rho),$$

$$R_D(t_{\rho+1}) = R_D(t_\rho) + \tau_{D1} I_{D1}(t_\rho) + \tau_{D2} I_{D2}(t_\rho) - m_H R_D(t_\rho)$$

$$- \frac{\beta_C I_C(\rho)}{N_H(t_\rho)} R_D(t_\rho) - \theta_D R_D(t_\rho),$$

$$R_C(t_{\rho+1}) = R_C(t_\rho) + \tau_C I_C(t_\rho) - m_H R_C(t_\rho) - \theta_C R_C(t_\rho)$$

$$+ \left(\frac{\beta_{V2} I_{V2}(t_\rho)}{N_H(t_\rho)} + \frac{\beta_{V1} I_{V1}(t_\rho)}{N_H(t_\rho)} \right) R_C(t_\rho),$$

$$S_V(t_{\rho+1}) = S_V(t_\rho) + \Lambda_V - \left(\frac{\beta_{D2}(I_{D2}(t_\rho) + I_{DC2}(t_\rho))}{N_H(t_\rho)} + \frac{\beta_{D1}(I_{D1}(t_\rho) + I_{DC1}(t_\rho))}{N_H(t_\rho)} \right)$$

$$S_V(t_\rho) - m_V S_V(t_\rho),$$

$$I_{V1}(t_{\rho+1}) = I_{V1}(t_\rho) + \frac{\beta_{D1}(I_{D1}(t_\rho) + I_{DC1}(t_\rho))}{N_H(t_\rho)} S_V(t_\rho) - m_V I_{V1}(t_\rho),$$

$$I_{V2}(t_{\rho+1}) = I_{V2}(t_\rho) + \frac{\beta_{D2}(I_{D2}(t_\rho) + I_{DC2}(t_\rho))}{N_H(t_\rho)} S_V(t_\rho) - m_V I_{V2}(t_\rho). \tag{9}$$

$$N_H(t_\rho) = R_D(t_\rho) + R_C(t_\rho) + I_C(t_\rho) + S_H(t_\rho) + I_{D1}(t_\rho)$$

$$+ I_{D2}(t_\rho) + I_{DC1}(t_\rho) + I_{DC2}(t_\rho).$$

The initial conditions:

$$I_{D1}(t_{\rho_0}) \geq 0,\ S_H(t_{\rho_0}) \geq 0,\ I_{D2}(t_{\rho_0}),\ I_{V1}(t_{\rho_0}) \geq 0,\ S_V(t_{\rho_0}) \geq 0,\ I_{V2}(t_{\rho_0}) \geq 0,$$

$$R_D(t_{\rho_0}) \geq 0,\ R_C(t_{\rho_0}) \geq 0,\ I_C(t_{\rho_0}) \geq 0,\ I_{DC1}(t_{\rho_0}) \geq 0,\ I_{DC2}(t_{\rho_0}) \geq 0. \tag{10}$$

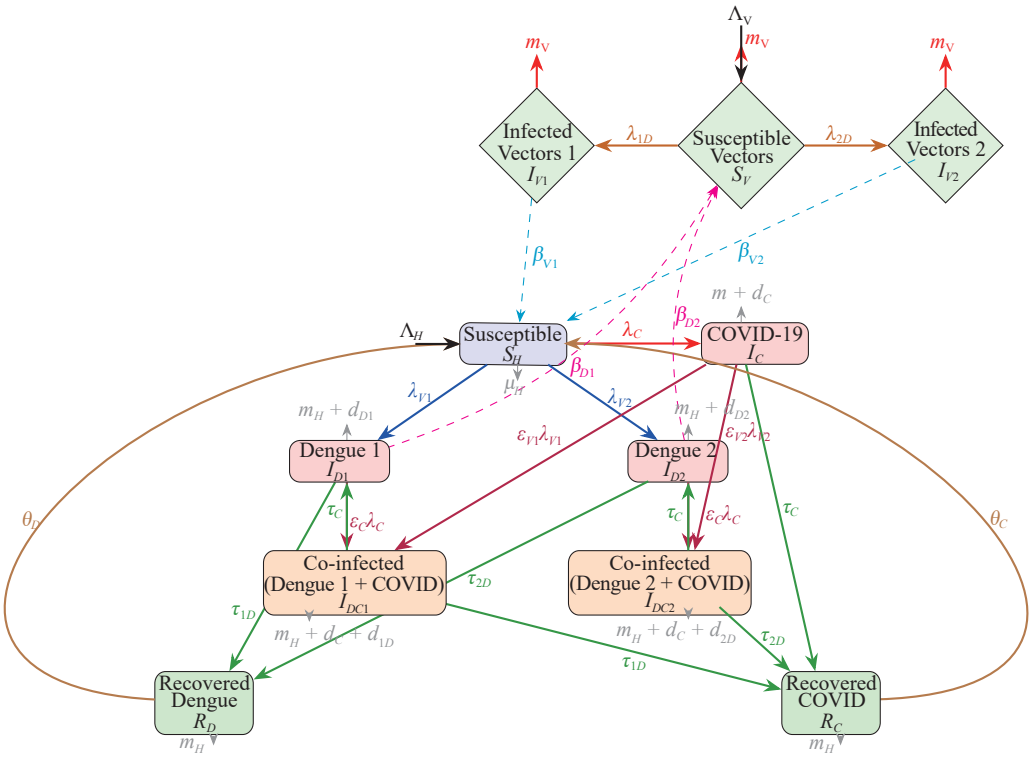

Figure 1. Compartmental diagram of the dengue-COVID-19 co-circulation model. The model includes two dengue strains (D1 and D2) and COVID-19, with co-infection possibilities

3.2 *Fractional-order discrete model*

The following is the first-order difference for the two strains of COVID-19 and dengue co-circulating epidemic model (9). This model is developed using the reference [33]. While [33] establishes a classical integer-order discrete-time model, our primary contribution here is its generalization to a Caputo fractional-order framework. This reformulation incorporates memory effects and non-local dynamics into the system, which are essential for accurately modeling the lingering impact of past infections, immunity waning, and intervention strategies. This fractional extension provides a more powerful and biologically relevant tool for capturing the complex temporal patterns of co-circulating epidemics, which is a central novel aspect of our study.

$$\triangle S_H(t_\rho) = \Lambda_H - \left(\frac{\beta_{V2} I_{V2}(t_\rho)}{N_H(t_\rho)} + \frac{\beta_C (I_{DC2}(t_\rho) + I_{DC1}(t_\rho) + I_C(t_\rho))}{N_H(t_\rho)} \right.$$

$$\left. + \frac{\beta_{V1} I_{V1}(t_\rho)}{N_H(t_\rho)} \right) S_H(t_\rho) - m_H S_H(t_\rho) + \theta_C R_C(t_\rho)$$

$$+ \theta_D R_D(t_\rho),$$

$$\triangle I_{D1}(t_\rho) = \frac{\beta_{V1} I_{V1}(t_\rho)}{N_H(t_\rho)} (S_H(t_\rho) + R_C(t_\rho)) - (\tau_{D1} + d_{D1} + m_H) I_{D1}(t_\rho)$$

$$- \varepsilon_C \frac{\beta_C (I_{DC2}(t_\rho) + I_{DC1}(t_\rho) + I_C(t_\rho))}{N_H(t_\rho)} I_{D1}(t_\rho)$$

$$+ \tau_C I_{DC1}(t_\rho),$$

$$\triangle I_{D2}(t_\rho) = \frac{\beta_{V2} I_{V2}(t_\rho)}{N_H(t_\rho)} (S_H(t_\rho) + R_C(t_\rho)) - (\tau_{D2} + d_{D2} + m_H) I_{D2}(t_\rho)$$

$$+ \varepsilon_C \frac{\beta_C (I_{DC2}(t_\rho) + I_{DC1}(t_\rho) + I_C(t_\rho))}{N_H(t_\rho)} I_{D2}(t_\rho)$$

$$+ \tau_C I_{DC2}(t_\rho + \zeta - 1),$$

$$\triangle I_C(t_\rho) = \frac{\beta_C (I_C(t_\rho) + I_{DC1}(t_\rho) + I_{DC2}(t_\rho))}{N_H(t_\rho)} (S_H(t_\rho) + R_D(\rho))$$

$$- (\tau_C + d_C + m_H) I_C(t_\rho) + \tau_{D1} I_{DC1}(t_\rho)$$

$$+ \tau_{D2} I_{DC2}(t_\rho) - \left(\varepsilon_{v2} \frac{\beta_{V2} I_{V2}(t_\rho)}{N_H(t_\rho)} + \varepsilon_{v1} \frac{\beta_{V1} I_{V1}(t_\rho)}{N_H(t_\rho)} \right) I_C(\rho),$$

$$\triangle I_{DC1}(t_\rho) = \varepsilon_C \frac{\beta_C (I_{DC2}(t_\rho) + I_{DC1}(t_\rho) + I_C(t_\rho))}{N_H(t_\rho)} I_{D1}(t_\rho)$$

$$+ \varepsilon_{v1} \frac{\beta_{V1} I_{V1}(t_\rho)}{N_H(t_\rho)} I_C(t_\rho) - (\tau_{D1} + d_{D1} + m_H + \tau_C + d_C) I_{D1}(t_\rho),$$

$$\triangle I_{DC2}(t_\rho) = \varepsilon_C \frac{\beta_C (I_{DC2}(t_\rho) + I_{DC1}(t_\rho) + I_C(t_\rho))}{N_H(t_\rho)} I_{D2}(t_\rho)$$

$$+ \varepsilon_{v2} \frac{\beta_{V2} I_{V2}(t_\rho)}{N_H(t_\rho)} I_C(t_\rho) - (\tau_{D2} + d_{D2} + m_H + \tau_C + d_C) I_{D2}(t_\rho),$$

$$\triangle R_D(t_\rho) = \tau_{D1} I_{D1}(t_\rho) + \tau_{D2} I_{D2}(t_\rho) - m_H R_D(t_\rho)$$

$$- \frac{\beta_C I_C(t_\rho)}{N_H(t_\rho)} R_D(t_\rho) - \theta_D R_D(t_\rho),$$

$$\triangle R_C(t_\rho) = \tau_C I_C(t_\rho) - m_H R_C(t_\rho) - \theta_C R_C(t_\rho)$$

$$+ \left(\frac{\beta_{V2} I_{V2}(t_\rho)}{N_H(t_\rho)} + \frac{\beta_{V1} I_{V1}(t_\rho)}{N_H(t_\rho)} \right) R_C(t_\rho),$$

$$\triangle S_V(t_\rho) = \Lambda_V - \left(\frac{\beta_{D2}(I_{D2}(t_\rho) + I_{DC2}(t_\rho))}{N_H(t_\rho)} + \frac{\beta_{D1}(I_{D1}(t_\rho) + I_{DC1}(t_\rho))}{N_H(t_\rho)} \right)$$

$$S_V(t_\rho) - m_V S_V(t_\rho),$$

$$\triangle I_{V1}(t_\rho) = \frac{\beta_{D1}(I_{D1}(t_\rho) + I_{DC1}(t_\rho))}{N_H(t_\rho)} S_V(t_\rho) - m_V I_{V1}(t_\rho),$$

$$I_{V2}(t_\rho) = I_{V2}(t_\rho) + \frac{\beta_{D2}(I_{D2}(t_\rho) + I_{DC2}(t_\rho))}{N_H(t_\rho)} S_V(t_\rho) - m_V I_{V2}(t_\rho). \tag{11}$$

We employ the Caputo-left difference operator (3) to develop the fractional discrete-time version. consider

$$\vartheta(t-1+\zeta) = \Big\{ S_H(t-1+\zeta),\, I_{D1}(t-1+\zeta),\, I_{D2}(t-1+\zeta),\, I_C(t+\zeta-1),\, I_{DC1}(t-1+\zeta),$$

$$I_{DC2}(t-1+\zeta),\, R_D(t-1+\zeta),\, R_C(t-1+\zeta),\, S_V(t-1+\zeta),\, I_{V1}(t-1+\zeta),\, I_{V2}(t-1+\zeta) \Big\}.$$

The new system of fractional-order Caputo difference with shifted time indices equations is defined as follows:

$${}^{C}\triangle_a^{\zeta} S_H = \Lambda_H - \left(\frac{\beta_{V2} I_{V2}(t+\zeta-1)}{N_H(t-1+\zeta)} \right.$$

$$+ \frac{\beta_C(I_{DC2}(t-1+\zeta) + I_{DC1}(t-1+\zeta) + I_C(t-1+\zeta))}{N_H(t-1+\zeta)}$$

$$\left. + \frac{\beta_{V1} I_{V1}(t-1+\zeta)}{N_H(t-1+\zeta)} \right) S_H(t-1+\zeta) - m_H S_H(t-1+\zeta) + \theta_C R_C(t-1+\zeta)$$

$$+ \theta_D R_D(t-1+\zeta) = \Upsilon_1(t-1+\zeta,\, \vartheta(t+\zeta-1)),$$

$$
\begin{aligned}
{}^{C}\triangle_{a}^{\zeta} I_{D1} &= (S_H(\zeta+t-1)\frac{\beta_{V1}I_{V1}(\zeta+t-1)}{N_H(t-1+\zeta)} + R_C(\zeta+t-1)) \\
&\quad -(\tau_{D1}+d_{D1}+m_H)I_{D1}(t-1+\zeta) \\
&\quad -\varepsilon_C\frac{\beta_C(I_{DC2}(t-1+\zeta)+I_{DC1}(t-1+\zeta)+I_C(t-1+\zeta))}{N_H(t-1+\zeta)}I_{D1}(t-1+\zeta) \\
&\quad +\tau_C I_{DC1}(t-1+\zeta) = \Upsilon_2(t-1+\zeta,\ \vartheta(t-1+\zeta)),
\end{aligned}
$$

$$
\begin{aligned}
{}^{C}\triangle_{a}^{\zeta} I_{D2} &= (S_H(\zeta+t-1)\frac{\beta_{V2}I_{V2}(\zeta+t-1)}{N_H(\zeta+t-1)} + R_C(\zeta+t-1)) \\
&\quad -(\tau_{D2}+d_{D2}+m_H)I_{D2}(\rho-1+\zeta) \\
&\quad +\varepsilon_C\frac{\beta_C(I_{DC2}(t-1+\zeta)+I_{DC1}(t-1+\zeta)+I_C(t-1+\zeta))}{N_H(t-1+\zeta)}I_{D2}(t-1+\zeta) \\
&\quad +\tau_C I_{DC2}(t-1+\zeta) = \Upsilon_3(t-1+\zeta,\ \vartheta(t-1+\zeta)),
\end{aligned}
$$

$$
\begin{aligned}
{}^{C}\triangle_{a}^{\zeta} I_{C} &= \frac{\beta_C(I_C(t-1+\zeta)+I_{DC1}(t-1+\zeta)+I_{DC2}(t-1+\zeta))}{N_H(t-1+\zeta)} \\
&\quad (S_H(t-1+\zeta)+R_D(t-1+\zeta)) \\
&\quad -(\tau_C+d_C+m_H)I_C(t-1+\zeta)+\tau_{D1}I_{DC1}(t-1+\zeta) \\
&\quad +\tau_{D2}I_{DC2}(t-1+\zeta)-\left(\varepsilon_{v2}\frac{\beta_{V2}I_{V2}(t-1+\zeta)}{N_H(t-1+\zeta)}+\varepsilon_{v1}\frac{\beta_{V1}I_{V1}(t-1+\zeta)}{N_H(t-1+\zeta)}\right) \\
&\quad I_C(t-1+\zeta) = \Upsilon_4(t-1+\zeta,\ \vartheta(t-1+\zeta)),
\end{aligned}
$$

$$
\begin{aligned}
{}^{C}\triangle_{a}^{\zeta} I_{DC1} &= \varepsilon_C\frac{\beta_C(I_{DC2}(t-1+\zeta)+I_{DC1}(t-1+\zeta)+I_C(t-1+\zeta))}{N_H(t-1+\zeta)} \\
&\quad I_{D1}(t-1+\zeta)+\varepsilon_{v1}\frac{\beta_{V1}I_{V1}(t-1+\zeta)}{N_H(t-1+\zeta)}I_C(t-1+\zeta) \\
&\quad -(\tau_{D1}+d_{D1}+m_H+\tau_C+d_C)I_{D1}(\rho-1+\zeta) = \Upsilon_5(t-1+\zeta,\ \vartheta(t-1+\zeta)),
\end{aligned}
$$

$$
\begin{aligned}
{}^{C}\triangle_{a}^{\zeta} I_{DC2} &= \varepsilon_C \frac{\beta_C (I_{DC2}(t-1+\zeta) + I_{DC1}(t-1+\zeta) + I_C(t-1+\zeta))}{N_H(t-1+\zeta)} I_{D2}(t-1+\zeta) \\
&\quad + \varepsilon_{v2} \frac{\beta_{V2} I_{V2}(t-1+\zeta)}{N_H(t-1+\zeta)} I_C(t-1+\zeta) - (\tau_{D2} + d_{D2} + m_H + \tau_C + d_C) \\
&\quad I_{D2}(t-1+\zeta) = \Upsilon_6(t-1+\zeta,\ \vartheta(t+\zeta-1)),
\end{aligned}
$$

$$
\begin{aligned}
{}^{C}\triangle_{a}^{\zeta} R_D &= \tau_{D1} I_{D1}(t-1+\zeta) + \tau_{D2} I_{D2}(t-1+\zeta) - m_H R_D(t-1+\zeta) \\
&\quad - \frac{\beta_C I_C(t-1+\zeta)}{N_H(t-1+\zeta)} R_D(t-1+\zeta) - \theta_D R_D(t-1+\zeta) = \Upsilon_7(t-1+\zeta,\ \vartheta(t-1+\zeta)),
\end{aligned}
$$

$$
\begin{aligned}
{}^{C}\triangle_{a}^{\zeta} R_C &= \tau_C I_C(t-1+\zeta) - m_H R_D(t-1+\zeta) - \theta_C R_C(t+\zeta-1) \\
&\quad + \left(\frac{\beta_{V2} I_{V2}(t+\zeta-1)}{N_H(t-1+\zeta)} + \frac{\beta_{V1} I_{V1}(t-1+\zeta)}{N_H(t-1+\zeta)} \right) R_C(t-1+\zeta) \\
&= \Upsilon_8(t-1+\zeta,\ \vartheta(t-1+\zeta)),
\end{aligned}
$$

$$
\begin{aligned}
{}^{C}\triangle_{a}^{\zeta} S_V &= \Lambda_V - \left(\frac{\beta_{D2} (I_{D2}(t-1+\zeta) + I_{DC2}(t-1+\zeta))}{N_H(t-1+\zeta)} \right. \\
&\quad \left. + \frac{\beta_{D1} (I_{D1}(t-1+\zeta) + I_{DC1}(t-1+\zeta))}{N_H(t-1+\zeta)} \right) \\
&\quad S_V(t-1+\zeta) - m_V S_V(t-1+\zeta) = \Upsilon_9(t-1+\zeta,\ \vartheta(t-1+\zeta)),
\end{aligned}
$$

$$
\begin{aligned}
{}^{C}\triangle_{a}^{\zeta} I_{V1} &= \frac{\beta_{D1} (I_{D1}(t-1+\zeta) + I_{DC1}(t-1+\zeta))}{N_H(t-1+\zeta)} S_V(t-1+\zeta) - m_V I_{V1}(t-1+\zeta) \\
&= \Upsilon_{10}(t+\zeta-1,\ \vartheta(t-1+\zeta)),
\end{aligned}
$$

$$
\begin{aligned}
{}^{C}\triangle_{a}^{\zeta} I_{V2} &= \frac{\beta_{D2} (I_{D2}(t-1+\zeta) + I_{DC2}(t-1+\zeta))}{N_H(t-1+\zeta)} S_V(t-1+\zeta) - m_V I_{V2}(t-1+\zeta) \\
&= \Upsilon_{11}(t-1+\zeta,\ \vartheta(t-1+\zeta)).
\end{aligned} \tag{12}
$$

$$N_H(t-1+\zeta) = R_D(t-1+\zeta) + R_C(t-1+\zeta) + I_C(t-1+\zeta) + S_H(t-1+\zeta) + I_{D1}(t-1+\zeta)$$

$$+ I_{D2}(t-1+\zeta) + I_{DC1}(\rho-1+\zeta) + I_{DC2}(t-1+\zeta).$$

The initial conditions:

$$I_{D1}(t_0) \geq 0,\ S_H(t_0) \geq 0,\ I_{D2}(t_0),\ I_{V1}(t_0) \geq 0,\ S_V(t_0) \geq 0,\ I_{V2}(t_0) \geq 0,$$

$$R_D(t_0) \geq 0,\ R_C(t_0) \geq 0,\ I_C(t_0) \geq 0,\ I_{DC1}(t_0) \geq 0,\ I_{DC2}(t_0) \geq 0. \tag{13}$$

3.3 *Variable-order discrete time model*

We will extend the Caputo-left difference operator (3) to a variable-order discrete model, the new system of variable-order Caputo difference with shifted time indices equations [22] defined as follows:

$$\begin{aligned}
{}^{C}\triangle_a^{\zeta(t)} S_H &= \Lambda_H - \left(\frac{\beta_{V2} I_{V2}(t-1+\zeta(t))}{N_H(t-1+\zeta(t))} \right. \\
&\quad + \frac{\beta_C (I_{DC2}(t-1+\zeta(t)) + I_{DC1}(t-1+\zeta(t)) + I_C(t-1+\zeta(t)))}{N_H(t-1+\zeta(t))} \\
&\quad \left. + \frac{\beta_{V1} I_{V1}(t-1+\zeta(t))}{N_H(t-1+\zeta(t))} \right) S_H(t-1+\zeta(t)) - m_H S_H(t-1+\zeta(t)) \\
&\quad + \theta_C R_C(t-1+\zeta(t)) + \theta_D R_D(t-1+\zeta(t)), \\
{}^{C}\triangle_a^{\zeta(t)} I_{D1} &= \frac{\beta_{V1} I_{V1}(t-1+\zeta(t))}{N_H(t-1+\zeta(t))} (S_H(t-1+\zeta(t)) + \\
&\quad R_C(t-1+\zeta(t))) - (\tau_{D1} + d_{D1} + m_H) I_{D1}(t-1+\zeta(t)) \\
&\quad - \varepsilon_C \frac{\beta_C (I_{DC2}(t-1+\zeta(t)) + I_{DC1}(t-1+\zeta(t)) + I_C(t-1+\zeta(t)))}{N_H(t-1+\zeta(t))} \\
&\quad I_{D1}(t-1+\zeta(t)) + \tau_C I_{DC1}(t-1+\zeta(t)),
\end{aligned}$$

$$
{}^{C}\triangle_{a}^{\zeta(t)} I_{D2} = \frac{\beta_{V2} I_{V2}(t-1+\zeta(t))}{N_H(t-1+\zeta(t))}(S_H(t-1+\zeta(t))
$$

$$
+ R_C(t-1+\zeta(t))) - (\tau_{D2} + d_{D2} + m_H) I_{D2}(t-1+\zeta(t))
$$

$$
+ \varepsilon_C \frac{\beta_C(I_{DC2}(t+\zeta(t)-1) + I_{DC1}(t-1+\zeta(t)) + I_C(t-1+\zeta(t)))}{N_H(t-1+\zeta(t))}
$$

$$
I_{D2}(\rho - 1 + \zeta(t)) + \tau_C I_{DC2}(t-1+\zeta(t)),
$$

$$
{}^{C}\triangle_{a}^{\zeta(t)} I_C = \frac{\beta_C(I_C(t-1+\zeta(t)) + I_{DC1}(t-1+\zeta(t)) + I_{DC2}(t-1+\zeta(t)))}{N_H(t-1+\zeta(t))}
$$

$$
(S_H(t-1+\zeta(t)) + R_D(t-1+\zeta(t)))
$$

$$
- (\tau_C + d_C + m_H) I_C(t-1+\zeta(t)) + \tau_{D1} I_{DC1}(t-1+\zeta(t))
$$

$$
+ \tau_{D2} I_{DC2}(t-1+\zeta(t)) - \left(\varepsilon_{v2} \frac{\beta_{V2} I_{V2}(t-1+\zeta(t))}{N_H(t-1+\zeta(t))}\right.
$$

$$
\left. + \varepsilon_{v1} \frac{\beta_{V1} I_{V1}(t-1+\zeta(t))}{N_H(t-1+\zeta(t))}\right) I_C(t-1+\zeta(t)),
$$

$$
{}^{C}\triangle_{a}^{\zeta(t)} I_{DC1} = \varepsilon_C \frac{\beta_C(I_{DC2}(t-1+\zeta(t)) + I_{DC1}(t-1+\zeta(t)) + I_C(t-1+\zeta(t)))}{N_H(t-1+\zeta(t))}
$$

$$
I_{D1}(t-1+\zeta(t)) + \varepsilon_{v1} \frac{\beta_{V1} I_{V1}(t-1+\zeta(t))}{N_H(t-1+\zeta(t))} I_C(t-1+\zeta(t))
$$

$$
- (\tau_{D1} + d_{D1} + m_H + \tau_C + d_C) I_{D1}(t-1+\zeta(t)),
$$

$$
{}^{C}\triangle_{a}^{\zeta(t)} I_{DC2} = \varepsilon_C \frac{\beta_C(I_{DC2}(t-1+\zeta(t)) + I_{DC1}(t-1+\zeta(t)) + I_C(t+\zeta(t)-1))}{N_H(t-1+\zeta(t))}
$$

$$
I_{D2}(t-1+\zeta(t)) + \varepsilon_{v2} \frac{\beta_{V2} I_{V2}(t-1+\zeta(t))}{N_H(t-1+\zeta(t))} I_C(t-1+\zeta(t))
$$

$$
- \left(\tau_{D2} + d_{D2} + m_H + \tau_C + d_C\right) I_{D2}(t-1+\zeta(t)),
$$

$$
\begin{aligned}
{}^{C}\triangle_{a}^{\zeta(\rho)} R_D &= \tau_{D1} I_{D1}(t-1+\zeta(t)) + \tau_{D2} I_{D2}(t-1+\zeta(t)) - m_H R_D(t-1+\zeta(t)) \\
&\quad - \frac{\beta_C I_C(t-1+\zeta(t))}{N_H(t+\zeta(t)-1)} R_D(t-1+\zeta(t)) - \theta_D R_D(t-1+\zeta(t)), \\
{}^{C}\triangle_{a}^{\zeta(t)} R_C &= \tau_C I_C(t-1+\zeta(t)) - m_H R_D(t-1+\zeta(t)) - \theta_C R_C(t-1+\zeta(t)) \\
&\quad + \left(\frac{\beta_{V2} I_{V2}(t-1+\zeta(t))}{N_H(t-1+\zeta(t))} + \frac{\beta_{V1} I_{V1}(t-1+\zeta(t))}{N_H(t-1+\zeta(t))} \right) R_C(t-1+\zeta(t)), \\
{}^{C}\triangle_{a}^{\zeta(t)} S_V &= \Lambda_V - \left(\frac{\beta_{D2}(I_{D2}(t-1+\zeta(t)) + I_{DC2}(t-1+\zeta(t)))}{N_H(t-1+\zeta(t))} \right. \\
&\quad \left. + \frac{\beta_{D1}(I_{D1}(t-1+\zeta(t)) + I_{DC1}(t-1+\zeta(t)))}{N_H(t-1+\zeta(t))} \right) \\
&\quad S_V(t-1+\zeta(t)) - m_V S_V(t-1+\zeta(t)), \\
{}^{C}\triangle_{a}^{\zeta(t)} I_{V1} &= \frac{\beta_{D1}(I_{D1}(t-1+\zeta(t)) + I_{DC1}(t-1+\zeta(t)))}{N_H(t-1+\zeta(t))} S_V(t-1+\zeta(t)) \\
&\quad - m_V I_{V1}(t-1+\zeta(t)), \\
{}^{C}\triangle_{a}^{\zeta(t)} I_{V2} &= \frac{\beta_{D2}(I_{D2}(t+\zeta(t)-1) + I_{DC2}(t-1+\zeta(t)))}{N_H(t-1+\zeta(t))} S_V(t-1+\zeta(t)) \\
&\quad - m_V I_{V2}(t-1+\zeta(t)).
\end{aligned} \tag{14}
$$

$$
\begin{aligned}
N_H(t+\zeta(t)-1) &= R_D(t+\zeta(t)-1) + R_C(t+\zeta(t)-1) + I_C(t+\zeta(t)-1) \\
&\quad + S_H(t+\zeta(t)-1) + I_{D1}(t+\zeta(t)-1) \\
&\quad + I_{D2}(t+\zeta(t)-1) + I_{DC1}(t+\zeta(t)-1) + I_{DC2}(t+\zeta(t)-1).
\end{aligned}
$$

Table 3 shows summary and comparison of the proposed discrete-time epidemiological models.

Table 3. Summary and comparison of the proposed discrete-time epidemiological models

Model	Description	Key features/Operators	Eq. No.
Integer-Order	A classical discrete-time model for co-circulation of two dengue strains and COVID-19	• Standard difference operator • Includes co-infection compartments • Serves as a baseline model	(9)
Fractional-Order (Constant)	Caputo fractional-order generalization of Model (9) with fixed memory length	• Constant order Caputo difference operator ${}^{C}\Delta_a^{\zeta}$ • Captures memory effects • $\zeta \in (0,\ 1]$ is constant	(11)
Variable-Order	Extension of the fractional model with time-dependent memory effects	• Variable order Caputo operator ${}^{C}\Delta_a^{\zeta(t)}$ • Memory length evolves with time • Adapts to changing epidemic phases	(14)
Crossover models	Hybrid models combining fixed and variable-order operators in different time intervals	• 1st Crossover: (12) for $t \leq t_1$, then (14) for $t > t_1$ • 2nd Crossover: (14) for $t \leq t_1$, then (12) for $t > t_1$ • Captures regime shifts in dynamics	(12) & (14)

3.4 *Parameter estimation and model calibration*

To ensure the biological relevance of our fractional-order model, we calibrate the parameters using real epidemiological data from regions experiencing dengue-COVID-19 co-circulation. We employ maximum likelihood estimation to fit the model to reported case counts from [Data Source, e.g., Brazilian health authorities] [34].

The calibration process minimizes the objective function:

$$\mathscr{J}(\theta) = \sum_{t=1}^{T} \|\mathbf{y}_{\text{data}}(t) - \mathbf{y}_{\text{model}}(t,\ \theta)\|^2,$$

where $\theta = \{\zeta,\ \beta_{V1},\ \beta_{V2},\ \beta_C,\ \tau_{D1},\ \tau_{D2},\ \tau_C,\ \ldots\}$ represents the parameter vector, $\mathbf{y}_{\text{data}}(t)$ are observed case counts, and $\mathbf{y}_{\text{model}}(t,\ \theta)$ are model predictions.

The fractional order ζ is estimated alongside biological parameters, allowing the memory effects to be informed by the temporal structure of the empirical data. This data-driven approach ensures our model captures real-world transmission dynamics rather than relying solely on theoretical assumptions.

4. Analysis of the proposed models

Lemma 2 (Positivity of the Solution) Assume that all initial conditions of the discrete-time epidemic system (12) are non-negative. Then, the solution of the system remains non-negative for all subsequent time steps, i.e.,

$$X_n \geq 0 \quad \text{for all} \quad n \geq 0.$$

Proof. Consider the fractional-order system (12) written in the vector form:

$${}^{C}\Delta_a^{\zeta}\mathbf{X}(t) = \mathbf{F}(t+\zeta-1,\ \mathbf{X}(t+\zeta-1)),$$

where $\mathbf{X}(t) = (S_H(t),\ I_{D1}(t),\ \ldots,\ I_{V2}(t))^T$ is the state vector and $\mathbf{F} = (T_1,\ T_2,\ \ldots,\ T_{11})^T$ is the vector-valued function defined in (12).

According to the discrete fractional calculus theory (Theorem 1 and the equivalent integral equation (7)), the unique solution to this system is given by:

$$\mathbf{X}(t) = \mathbf{X}(a) + \frac{1}{\Gamma(\zeta)} \sum_{\tau=a+1-\zeta}^{t-\zeta} (t-\tau-1)^{(\zeta-1)} \mathbf{F}(\tau+\zeta-1,\ \mathbf{X}(\tau+\zeta-1)),$$

for $t \in \mathbb{N}_{a+1}$. For the initial point $a = 0$ and shifting the index by letting $n = t$, $k = \tau + 1$, this solution can be rewritten in the following recursive form for $n \geq 0$:

$$\mathbf{X}_{n+1} = \mathbf{X}_0 + \frac{1}{\Gamma(\zeta)} \sum_{k=1}^{n+1} \frac{\Gamma(n-k+\zeta+1)}{\Gamma(n-k+2)} \mathbf{F}_{k-1}(\mathbf{X}),$$

where $\mathbf{X}_n = \mathbf{X}(n)$ and $\mathbf{F}_k(\mathbf{X}) = \mathbf{F}(k,\ \mathbf{X}(k))$.

We now prove the positivity by induction. The base case is given by the non-negative initial conditions: $\mathbf{X}_0 \geq 0$.

For the inductive step, assume $\mathbf{X}_k \geq 0$ for all $k \leq n$. We must show that $\mathbf{X}_{n+1} \geq 0$. Examining the numerical formula:

$$\mathbf{X}_{n+1} = \mathbf{X}_0 + \frac{1}{\Gamma(\zeta)} \sum_{k=1}^{n+1} \underbrace{\frac{\Gamma(n-k+\zeta+1)}{\Gamma(n-k+2)}}_{w_{n,\ k}} \mathbf{F}_{k-1}(\mathbf{X}),$$

we note that the weights $w_{n,\ k} > 0$ for $\zeta \in (0,\ 1]$ because the Gamma function is positive for positive arguments.

The crucial step is to analyze the function $\mathbf{F}$. By direct inspection of the components $T_1,\ \ldots,\ T_{11}$ in system (12), we observe that the right-hand side $\mathbf{F}(\cdot,\ \mathbf{X})$ has the following structure for each compartment X^i:

$$T_i(t,\ \mathbf{X}) = \Lambda_i + \sum_j \alpha_{ij}(t,\ \mathbf{X}) X^j - \phi_i(t,\ \mathbf{X}) X^i,$$

where $\Lambda_i \geq 0$ is a constant recruitment term (if it exists for the compartment), $\alpha_{ij}(t,\ \mathbf{X}) \geq 0$ are non-negative coupling coefficients representing inflows from other compartments, and $\phi_i(t,\ \mathbf{X}) \geq 0$ is the total rate of outflow from compartment X^i.

A key biological feature is that the outflow term $\phi_i(t,\ \mathbf{X})X^i$ vanishes when $X^i = 0$. Therefore, if at any step $\mathbf{X}_k \geq 0$, then $\mathbf{F}_k(\mathbf{X}) \geq 0$ because the negative terms are multiplicative in the state variables and thus zero if the state is zero. By the induction hypothesis, $\mathbf{X}_k \geq 0$ for $k \leq n$, so $\mathbf{F}_{k-1}(\mathbf{X}) \geq 0$ for $k = 1,\ \ldots,\ n+1$.

Since $\mathbf{X}_0 \geq 0$, all weights $w_{n,\ k} > 0$, and all $\mathbf{F}_{k-1}(\mathbf{X}) \geq 0$, it follows that every term in the sum is non-negative. Consequently, $\mathbf{X}_{n+1} \geq 0$.

By the principle of mathematical induction, the solution $\mathbf{X}_n \geq 0$ for all $n \geq 0$. □

Proposition 3 (Boundedness of the Solution) Let all initial conditions of the discrete-time fractional epidemic system be non-negative and finite. Then the solution remains bounded for all time steps $n \geq 0$.

Proof. Let $N_H(n)$ and $N_V(n)$ denote the total human and vector populations at time step n, respectively. Summing the human compartmental equations yields a recursive inequality:

$$N_H(n+1) \leq N_H(1) + \sum_{k=1}^{n} w_{n,\,k} \cdot (A_H - m_H N_H(k)),$$

where $w_{n,\,k} = \Gamma(n-k+\alpha)/\Gamma(n-k+1) > 0$ are fractional weights. By bounding the terms, we deduce:

$$N_H(n) \leq \max\left\{N_H(1),\ \frac{A_H}{m_H}\right\}.$$

An analogous argument applies for the vector population, giving:

$$N_V(n) \leq \max\left\{N_V(1),\ \frac{A_V}{m_V}\right\}.$$

Since each compartment represents a non-negative subset of the total population and the model ensures positivity, all state variables remain bounded above by a finite constant M. Thus, the solution is bounded for all $n \geq 0$. □

4.1 *The basic reproduction number*

The Disease-Free Equilibrium (DFE) is obtained by setting both the infected variable and the right-hand sides of the model (11) to zero.

$$\Xi_0 = \left(\breve{S_H},\ 0,\ 0,\ 0,\ 0,\ 0,\ 0,\ 0,\ \breve{S_V},\ 0,\ 0\right)$$

$$= \left((m_H)^{-1}\Lambda_H,\ 0,\ 0,\ 0,\ 0,\ 0,\ 0,\ 0,\ (m_V)^{-1}\Lambda_V,\ 0,\ 0\right).$$

The next-generation matrix is applied to the model (11) to analyze the DFE's stability. Below are the corresponding transfer matrices:

$$F = \begin{pmatrix} 0 & 0 & 0 & 0 & 0 & \beta_{V1} & 0 \\ 0 & 0 & 0 & 0 & 0 & 0 & \beta_{V2} \\ 0 & 0 & \beta_C & \beta_C & \beta_C & 0 & 0 \\ 0 & 0 & 0 & 0 & 0 & 0 & 0 \\ 0 & 0 & 0 & 0 & 0 & 0 & 0 \\ \beta_{D1}(\breve{S_H})^{-1}\breve{S_V} & 0 & 0 & \beta_{D1}(\breve{S_H})^{-1}\breve{S_V} & 0 & 0 & 0 \\ 0 & \beta_{D2}(\breve{S_H})^{-1}\breve{S_V} & 0 & 0 & \beta_{D2}(\breve{S_H})^{-1}\breve{S_V} & 0 & 0 \end{pmatrix}.$$

$$V = \begin{pmatrix} J_1 & 0 & 0 & J_{11} & 0 & 0 & 0 \\ 0 & J_2 & 0 & 0 & J_{11} & 0 & 0 \\ 0 & 0 & J_3 & J_{22} & J_{33} & 0 & 0 \\ 0 & 0 & 0 & J_4 & 0 & 0 & 0 \\ 0 & 0 & 0 & 0 & J_5 & 0 & 0 \\ 0 & 0 & 0 & 0 & 0 & 1-m_V & 0 \\ 0 & 0 & 0 & 0 & 0 & 0 & 1-m_V \end{pmatrix}.$$

Where,

$$J_1 = 1 - m_H + d_{D1} + \tau_{D1}, \quad J_{11} = -\tau_C, \quad J_2 = 1 - m_H + d_{D1} + \tau_{D1}, \quad J_{22} = \tau_{D1}, \quad J_{33} = -\tau_{D2},$$

$$J_4 = 1 - m_H + d_{D1} + \tau_{D1} + d_C + \tau_C, \quad J_5 = 1 - m_H + d_{D2} + \tau_{D2} + d_C + \tau_C.$$

R_0 corresponds to the spectral radius (or dominant eigenvalue) of the next-generation matrix.

$$K = F(I-V)^{-1}.$$

The basic reproduction number R_0 is defined as the spectral radius of the next-generation matrix:

$$R_0 = \rho\left(F(I-V)^{-1}\right),$$

where F and V are the new infection and transition matrices, respectively.

$$R_0 = \max\left\{R_{0,\,D1},\, R_{0,\,D2},\, R_{0,\,C}\right\}.$$

Using the disease-free equilibrium values $\breve{S_H} = \dfrac{\Lambda_H}{m_H}$ and $\breve{S_V} = \dfrac{\Lambda_V}{m_V}$, we define the reproduction numbers of the individual pathways as follows:

$$R_{0,\,D1} = \left[\frac{\beta_{V1}\beta_{D1}\Lambda_V m_H}{(1-m_V)\,m_V\,\Lambda_H\,(J_1J_4 - J_{11}\tau_C)}\right]^{1/2},$$

$$R_{0,\,D2} = \left[\frac{\beta_{V2}\beta_{D2}\Lambda_V m_H}{(1-m_V)\,m_V\,\Lambda_H\,(J_2J_5 - J_{11}\tau_C)}\right]^{1/2},$$

$$R_{0,\,C} = \frac{\beta_C}{J_4}.$$

4.2 *The model's disease-free equilibrium: local stability*

Theorem 2 The model's DFE (Ξ_0) is locally asymptotically stable whenever $R_0 < 1$ and unstable when $R_0 > 1$, [16, 35].

Proof. Using the Jacobian matrix of system (11) evaluated at the DFE, which is provided by:

$$J(\Xi_0) = \begin{pmatrix}
\Lambda_H & 0 & 0 & -\beta_C & -\beta_C & -\beta_C & \theta_D & \theta_C & 0 & -\beta_{V1} & -\beta_{V2} \\
0 & -J_1 & 0 & 0 & \tau_C & 0 & 0 & 0 & 0 & \beta_{V1} & 0 \\
0 & 0 & -J_2 & 0 & 0 & \tau_C & 0 & 0 & 0 & & \beta_{V2} \\
0 & 0 & 0 & -J_3+\beta_C\tau_{D1} & 0 & 0 & 0 & 0 & 0 & 0 & \\
 & & & +B_C+\beta_C\tau_{D2} & & & & & & & \\
0 & 0 & 0 & 0 & -J_4 & 0 & 0 & 0 & 0 & 0 & 0 \\
0 & 0 & 0 & 0 & 0 & -J_5 & 0 & 0 & 0 & 0 & 0 \\
0 & \tau_{D1} & \tau_{D2} & 0 & 0 & 0 & -m_H-\theta_D & & 0 & 0 & 0 \\
0 & 0 & 0 & \tau_C & 0 & 0 & 0 & -m_H-\theta_C & 0 & 0 & 0 \\
0 & -\frac{\beta_{D1}\check{S}_V}{\check{S}_H} & -\frac{\beta_{D2}\check{S}_V}{\check{S}_H} & 0 & -\frac{\beta_{D1}\check{S}_V}{\check{S}_H} & -\frac{\beta_{D2}\check{S}_V}{\check{S}_H} & 0 & 0 & -m_V & 0 & 0 \\
0 & \frac{\beta_{D1}\check{S}_V}{\check{S}_H} & 0 & 0 & \frac{\beta_{D1}\check{S}_V}{\check{S}_H} & 0 & 0 & & 0 & -m_V & 0 \\
0 & 0 & \frac{\beta_{D2}\check{S}_V}{\check{S}_H} & 0 & 0 & \frac{\beta_{D2}\check{S}_V}{\check{S}_H} & 0 & & 0 & 0 & 0 & -m_V
\end{pmatrix}.$$

The eigenvalues are presented below: $\eta_1 = 1-m_H$, $\eta_2 = 1-m_V$, $\eta_3 = -(-1+d_{D1}+m_H+\tau_C+d_C+\tau_{D1})$, $\eta_4 = -(-1+d_{D1}+m_H+\tau_C+d_C+\tau_{D2})$, $\eta_5 = 1-(\theta_C+m_H)$, $\eta_6 = 1-(\theta_D+m_H)$. The remaining eigenvalues are derived from the characteristic polynomial equations.

$$\eta + J_3(1-R_{0,\,C}) = 0,$$

$$\eta^2 + m_V J_1 \eta + m_V J_1 (1-R_{0,\,D1}^2) = 0,$$

$$\eta^2 + m_V J_2 \eta + m_V J_2 (1-R_{0,\,D2}^2) = 0.$$

According to the Routh-Hurwitz criterion, the above three equations will have roots with negative real portions if the related reproduction numbers $R_{0,\,C}$, $R_{0,\,D1}$, and $R_{0,\,D2}$, are less than one. Local asymptotic stability of the DFE is maintained when the reproduction number increases. If $R_0 > 1$, then

$$R_0 = \max\{R_{0,\,D1},\, R_{0,\,D2},\, R_{0,\,C}\} < 1.$$

Additionally, for $i = 0,\ 1,\ 2,\ \ldots,\ 11$, $|arg\eta_i| > 0.5\pi\mu$, $\mu \in (0,\ 1)$, and $Im(\eta_i) = 0$. □

4.3 *Discussion of the sensitivity analysis*

The bar chart in Figure 2 illustrates the sensitivity indices of key parameters affecting the basic reproduction number (R_0) within the proposed epidemic model, offering quantitative insights into their relative influence on disease transmission dynamics. Among these, the transmission rate β_C emerges as the most dominant factor, with a sensitivity index approaching unity, confirming its pivotal role in driving the epidemic potential. This finding highlights the critical need for control measures-such as vaccination campaigns, social distancing, and mask mandates targeted at reducing β_C. Conversely, the recovery rate τ_C displays a pronounced negative sensitivity index, indicating that improvements in treatment and patient recovery can significantly suppress R_0 and mitigate outbreak severity.

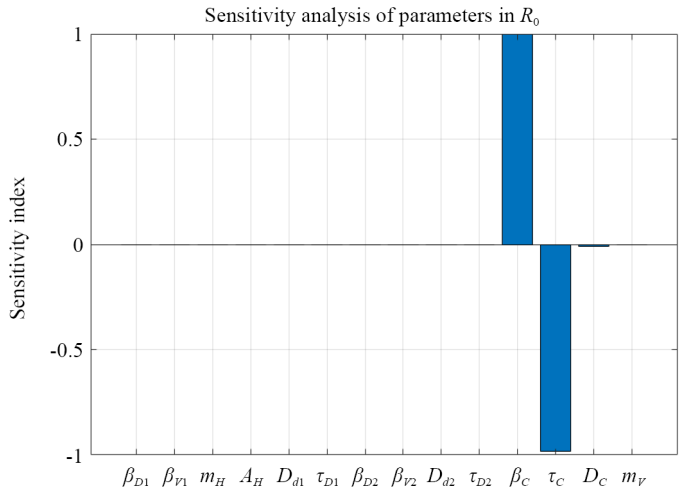

Figure 2. Visualize sensitivity indices in a bar chart

In contrast, parameters such as β_{D1}, β_{V1}, and the natural mortality rate m_H demonstrate negligible sensitivity values, suggesting a limited impact on disease dynamics and a lower priority for direct intervention. The broader sensitivity trend reveals that parameters with positive indices (e.g., β_C) tend to elevate R_0, whereas those with negative indices (e.g., τ_C) contribute to its reduction. These opposing effects underscore the necessity of targeted strategies focused on amplifying the influence of suppressive factors while minimizing the effects of amplifying ones.

From an epidemiological perspective, the analysis supports prioritizing resources toward controlling highly sensitive parameters, particularly through enhancing recovery rates and reducing transmission potential. Moreover, the relatively low sensitivity of certain parameters reflects the model's structural robustness, affirming its reliability for predictive analysis under a range of plausible epidemiological scenarios. Ultimately, sensitivity analysis not only strengthens model interpretation but also facilitates informed, evidence-based public health policy and decision-making by identifying the most effective levers for disease control.

The sensitivity analysis in Table 4 reveals that the basic reproduction number R_0 is overwhelmingly dominated by the COVID-19 parameters. The transmission rate β_C is the most influential factor (index = + 1.0), while the recovery rate τ_C is the most effective for control (index ≈ -0.98). All parameters related to the two dengue strains have a negligible effect (index ≈ 0), indicating that the initial epidemic growth is primarily driven by COVID-19 dynamics.

Table 4. Elasticity indices of the basic reproduction number R_0 with respect to the model parameters. A positive (negative) index indicates that R_0 increases (decreases) as the parameter increases

Parameter	Elasticity index
β_C	1.0000
τ_C	−0.9818
d_C	−0.0085
β_{V1}	0.0000
β_{D1}	0.0000
β_{V2}	0.0000
β_{D2}	0.0000
τ_{D1}	0.0000
τ_{D2}	0.0000
d_{D1}	0.0000
d_{D2}	0.0000
m_H	−0.0001
Λ_H	0.0000

5. Existence and uniqueness of solutions

In this section, we establish the existence and uniqueness of solutions for the system (13). To achieve this, we apply the conditions of Perov's theorem [36]. Before proceeding, we first present some necessary preliminary results related to generalized Banach spaces and Perov's fixed point theorem. For further details, readers are encouraged to consult reference [36].

Definition 4 Let $\mathfrak{Z}$ be a vector space over $\mathbb{K} = \mathbb{R}$ or $\mathbb{C}$. A generalized norm on $\mathfrak{Z}$ is a map [37]

$$\|\cdot\|_G : \mathfrak{Z} \longrightarrow [0, +\infty)^n$$

$$\mathfrak{u} \mapsto \|\mathfrak{u}\|_G = \begin{pmatrix} \|\mathfrak{u}\|_1 \\ \vdots \\ \|\mathfrak{u}\|_n \end{pmatrix}$$

the following characteristics

(i) For all $\mathfrak{u} \in \mathfrak{Z}$; if $\|\mathfrak{u}\|_G = 0_{\mathbb{R}^n_+}$, then $\mathfrak{u} = 0_{\mathfrak{Z}}$,

(ii) $\|\mathfrak{a}\mathfrak{u}\|_G = |\mathfrak{a}|\|\mathfrak{u}\|_G$ for all $\mathfrak{u} \in \mathfrak{Z}$ and $\mathfrak{a} \in \mathbb{K}$, and

(iii) $\|\mathfrak{u} + \omega\|_G \preccurlyeq \|\mathfrak{u}_1\|_G + \|\mathfrak{u}_2\|_G$ for all $\mathfrak{u}_1, \mathfrak{u}_2 \in \mathfrak{Z}$.

The pair $(\mathfrak{Z}, \|\cdot\|_G)$ is called a generalized normed space. Moreover, $(\mathfrak{Z}, \|\cdot\|_G)$ is called a Generalized Banach Space (GBS), if the vector-valued metric space generated by its vector-valued metric $\delta_G(\mathfrak{u}_1, \mathfrak{u}_2) = \|\mathfrak{u}_1 - \mathfrak{u}_2\|_G$ is complete.

Definition 5 A matrix $\amalg \in \mathscr{M}_{n\times n}(\mathbb{R}_+)$ is considered convergent to zero if its powers approach the zero matrix O_n as the exponent m tends to infinity. Formally:

$$\amalg^m \longrightarrow O_n, \quad \text{as} \quad m \longrightarrow \infty.$$

Here, O_n represents the $n \times n$ zero matrix.

Definition 6 An operator $\mathfrak{N} : \mathfrak{Z} \to \mathfrak{Z}$ on a generalized metric space [37] $(\mathfrak{Z}, \mathfrak{d}_G)$ is defined as an $\amalg$-contraction if there exists a matrix $\amalg \in \mathscr{M}_{n\times n}(\mathbb{R}_+)$ that converges to O_n, such that for all $\rho,\ v \in \mathfrak{Z}$, the following inequality holds:

$$\delta_G(\mathfrak{N}(\rho),\ \mathfrak{N}(v)) \preccurlyeq \amalg \mathfrak{d}_G(\rho,\ v).$$

The following result is Perov's extension of the Banach contraction principle.

Theorem 3 [36] Consider a complete generalized metric space $\mathfrak{Z}$. If $\mathfrak{N} : \mathfrak{Z} \longrightarrow \mathfrak{Z}$ is an M-contraction operator on $\mathfrak{Z}$, then $\mathfrak{N}$ necessarily has a unique fixed point within $\mathfrak{Z}$.

Now, looking that the system (13) can be rewriting in the following classical form

$$\begin{cases} {}^{C}\triangle_{a}^{\zeta} X(t) = \Upsilon(X(t)), \\ \qquad\qquad\qquad\qquad 0 < t < t_1 < \infty, \\ X(0) = X_0, \end{cases} \tag{15}$$

where, the vector

$$X_0 = (S_H,\ I_{D1}(0),\ I_{D2}(0),\ I_C(0),\ I_{DC1}(0),\ I_{DC2}(0),\ R_D(0),\ R_C(0),\ S_V(0),\ I_{V1}(0),\ I_{V2}(0))^T$$

and the operator Υ is defined above in (12).

Looking that the space $\mathfrak{Z} = \prod_{i=1}^{11} \ell_\infty(\mathbb{N}_b,\ \mathbb{R})$ becomes a generalized Banach space if we equip it with the following generalized norm

$$\|.\|_G : \mathfrak{Z} \longrightarrow \mathbb{R}_+^{11}$$

$$X \mapsto \|X\|_G = \begin{pmatrix} \|S_H\|_\infty \\ \|I_{D1}\|_\infty \\ \|I_{D2}\|_\infty \\ \|I_C\|_\infty \\ \|I_{DC1}\|_\infty \\ \|I_{DC2}\|_\infty \\ \|R_D\|_\infty \\ \|R_C\|_\infty \\ \|S_V\|_\infty \\ \|I_{V1}\|_\infty \\ \|I_{V2}\|_\infty \end{pmatrix}.$$

Where

$$\|\vartheta\|_\infty = \sup_{\rho\in\mathbb{N}_a} |\vartheta(\rho)|.$$

To establish the unique solvability of system (13), we convert it into a fixed point problem involving the operator $\mathfrak{N}$, which is defined by $\mathfrak{N} : \prod_{i=1}^{11} \ell_\infty(\mathbb{N}_a,\ \mathbb{R}) \to \prod_{i=1}^{11} \ell_\infty(\mathbb{N}_a,\ \mathbb{R})$

$$\mathfrak{N}(X(t_\rho)) = X(0) + \frac{1}{\Gamma(\zeta)} \sum_{i=1}^{\rho} \frac{\Gamma(\rho - i + \zeta)}{\Gamma(\rho - i + 1)} \Upsilon(X(i-1)). \tag{16}$$

The next lemma is needed.

Lemma 3 Suppose that there is a vector $\pi \in \mathbb{R}^{11}$ fulfills

$$\pi = \begin{pmatrix} \pi_1 \\ \pi_2 \\ \pi_3 \\ \pi_4 \\ \pi_5 \\ \pi_6 \\ \pi_7 \\ \pi_8 \\ \pi_9 \\ \pi_{10} \\ \pi_{11} \end{pmatrix} \succcurlyeq \frac{k}{\Gamma(\zeta)} \begin{pmatrix} \Lambda_H + (1-m_H)\pi_1 + \theta_C\pi_8 + \theta_C\pi_7 \\ \beta_{V1}\pi_1 + \pi_8 + \tau_C\pi_5 + (\varepsilon_C + \tau_{D1} + d_{D1} + m_H)\pi_2 \\ \beta_{V2}\pi_1 + \pi_8 + \tau_C\pi_6 + (\varepsilon_C + \tau_{D2} + d_{D2} + m_H)\pi_3 \\ \beta_C\pi_1 + \pi_7 + \tau_{D1}\pi_5 + \tau_{D2}\pi_6 + (\tau_C + d_C + m_H + \varepsilon_{v1} + \varepsilon_{v2})\pi_4 \\ \pi_5 + \varepsilon_{v1}\pi_4 + |\varepsilon_C - \tau_{D1} - d_{D1} - m_H - \tau_C - d_C|\pi_2 \\ \pi_6 + \varepsilon_{v2}\pi_4 + |\varepsilon_C - \tau_{D2} - d_{D2} - m_H - \tau_C - d_C|\pi_3 \\ \tau_{D1}\pi_2 + \tau_{D2}\pi_3 + (1 - m_H - \beta_{V2} - \theta_D)\pi_7 \\ \tau_C\pi_2 + m_H\pi_7 + (1 + \beta_{V1} + \beta_{V2} + \theta_C)\pi_8 \\ (1-m_V)\pi_9 \\ \beta_{D1}\pi_9 + m_V\pi_{10} \\ \beta_{D2}\pi_9 + m_V\pi_{11} \end{pmatrix}, \tag{17}$$

Consequently, the operator $\mathfrak{N}$ maps the generalized ball $\bar{B}(X_0,\ \pi) \subset \mathfrak{Z}$ back into itself.

Proof. Let $X \in \bar{B}(X_0,\ \Delta)$, then

$$\begin{aligned} \|\mathfrak{N}(X) - X_0\|_G &= \left\| \frac{1}{\Gamma(\zeta)} \sum_{i=1}^{\rho} \frac{\Gamma(\rho - i + \zeta)}{\Gamma(\rho - i + 1)} \Upsilon(i-1) \right\|_G \\ &\preccurlyeq \frac{1}{\Gamma(\zeta)} \sum_{i=1}^{\rho} \left\| \frac{\Gamma(\rho - i + \zeta)}{\Gamma(\rho - i + 1)} \Upsilon(i-1) \right\|_G \\ &\preccurlyeq \frac{k}{\Gamma(\zeta)} C_\Upsilon, \end{aligned}$$

where

$$k = \sum_{i=1}^{\rho} \left| \frac{\Gamma(\rho - i + \zeta)}{\Gamma(\rho - i + 1)} \right|,$$

and

$$C_{\Upsilon} = \|\Upsilon(X)\|_G \preccurlyeq \begin{pmatrix} \Lambda_H + (1 - m_H)\pi_1 + \theta_C \pi_8 + \theta_C \pi_7 \\ \beta_{V1}\pi_1 + \pi_8 + \tau_C \pi_5 + (\varepsilon_C + \tau_{D1} + d_{D1} + m_H)\pi_2 \\ \beta_{V2}\pi_1 + \pi_8 + \tau_C \pi_6 + (\varepsilon_C + \tau_{D2} + d_{D2} + m_H)\pi_3 \\ \beta_C \pi_1 + \pi_7 + \tau_{D1}\pi_5 + \tau_{D2}\pi_6 + (\tau_C + d_C + m_H + \varepsilon_{v1} + \varepsilon_{v2})\pi_4 \\ \pi_5 + \varepsilon_{v1}\pi_4 + |\varepsilon_C - \tau_{D1} - d_{D1} - m_H - \tau_C - d_C|\pi_2 \\ \pi_6 + \varepsilon_{v2}\pi_4 + |\varepsilon_C - \tau_{D2} - d_{D2} - m_H - \tau_C - d_C|\pi_3 \\ \tau_{D1}\pi_2 + \tau_{D2}\pi_3 + (1 - m_H - \beta_{V2} - \theta_D)\pi_7 \\ \tau_C \pi_2 + m_H \pi_7 + (1 + \beta_{V1} + \beta_{V2} + \theta_C)\pi_8 \\ (1 - m_V)\pi_9 \\ \beta_{D1}\pi_9 + m_V \pi_{10} \\ \beta_{D2}\pi_9 + m_V \pi_{11} \end{pmatrix}$$

□

Lemma 4 The operator Υ is a G-Lipschitz operator; ie., there exists a square matrix $\amalg \in \mathscr{M}_{11}(\mathbb{R}_+)$ such that

$$\|\Upsilon(X) - \Upsilon(\bar{X})\|_G \preccurlyeq \amalg \|X - \bar{X}\|_G.$$

Proof. Let $X = (S_H, I_{D1}, I_{D2}, I_C, I_{DC1}, I_{DC2}, R_D, R_C, S_V, I_{V1}, I_{V2})$, $\bar{X} = (\bar{S_H}, \bar{I_{D1}}, \bar{I_{D2}}, \bar{I_C}, \bar{I_{DC1}}, \bar{I_{DC2}}, \bar{R_D}, \bar{R_C}, \bar{S_V}, \bar{I_{V1}}, \bar{I_{V2}}) \in \bar{B}(X_0, \pi)$. Since

$$\left(\frac{\beta_{V2} I_{V2} + \beta_C (I_{DC2} + I_{DC1} + I_C) + \beta_{V1} I_{V1}}{N_H} \right) < 1,$$

we have

$$\|\Upsilon_1(X) - \Upsilon_1(\bar{X})\|_G \preccurlyeq (1 - m_H)\|S_H - \bar{S}_H\|_G + \theta_C\|R_C - \bar{R}_C\|_G$$

$$+ \theta_D\|R_D - \bar{R}_D\|_G.$$

By the same why, we have

$$\frac{\beta_{V1} I_{V1}}{N_H} < 1$$

$$\varepsilon_C \frac{\beta_C(I_{DC2} + I_{DC1} + I_C)}{N_H} < 1,$$

hence

$$\|\Upsilon_2(X) - \Upsilon_2(\bar{X})\|_G \preccurlyeq \beta_{V1}\|S_H - \bar{S}_H\|_G + \|R_C - \bar{R}_C\|_G + \tau_C\|I_{DC1} - \bar{I}_{DC1}\|_G$$

$$+ (\varepsilon_C + \tau_{D1} + d_{D1} + m_H)\|I_{D1} - \bar{I}_{D1}\|_G,$$

and

$$\|\Upsilon_3(X) - \Upsilon_3(\bar{X})\|_G \preccurlyeq \beta_{V2}\|S_H - \bar{S}_H\|_G + \|R_C - \bar{R}_C\|_G + \tau_c\|I_{DC2} - \bar{I}_{DC2}\|_G$$

$$+ (\varepsilon_C - \tau_{D2} - d_{D2} - m_H)\|I_{D2} - \bar{I}_{D2}\|_G,$$

$$\|\Upsilon_4(X) - \Upsilon_4(\bar{X})\|_G \preccurlyeq \beta_C\|S_H - \bar{S}_H\|_G + \|R_D - \bar{R}_D\|_G + \tau_{D1}\|I_{DC1} - \bar{I}_{DC1}\|_G$$

$$+ \tau_{D2}\|I_{DC2} - \bar{I}_{DC2}\|_G + (\tau_C + d_C + m_H + \varepsilon_{v1} + \varepsilon_{v2})\|I_C - \bar{I}_C\|_G,$$

$$\|\Upsilon_5(X) - \Upsilon_5(\bar{X})\|_G \preccurlyeq \|I_{DC1} - \bar{I}_{DC1}\|_G + \varepsilon_{v1}\|I_C - \bar{I}_C\|_G$$

$$+ |\varepsilon_C - \tau_{D1} - d_{D1} - m_H - \tau_C - d_C|\|I_{D1} - \bar{I}_{D1}\|_G,$$

$$\|\Upsilon_6(X) - \Upsilon_6(\bar{X})\|_G \preccurlyeq \|I_{DC2} - \bar{I}_{DC2}\|_G + \varepsilon_{v2}\|I_C - \bar{I}_C\|_G$$

$$+ |\varepsilon_C - \tau_{D2} - d_{D2} - m_H - \tau_C - d_C|\|I_{D2} - \bar{I}_{D2}\|_G,$$

$$\|\Upsilon_7(X) - \Upsilon_7(\bar{X})\|_G \preccurlyeq \tau_{D1}\|I_{D1} - \bar{I}_{D1}\|_G + \tau_{D2}\|I_{D2} - \bar{I}_{D2}\|_G$$

$$+ (1 - m_H - \beta_{V2} - \theta_D)\|R_D - \bar{R}_D\|_G,$$

$$\|\Upsilon_8(X)-\Upsilon_8(\bar{X})\|_G \preccurlyeq \tau_C\|I_C-\bar{I}_C\|_G+m_H\|R_D-\bar{R}_D\|_G$$

$$+(1+\beta_{V1}+\beta_{V2}+\theta_C)\|R_C-\bar{R}_C\|_G,$$

$$\|\Upsilon_9(X)-\Upsilon_9(\bar{X})\|_G \preccurlyeq (1-m_V)\|S_V-\bar{S}_V\|_G,$$

$$\|\Upsilon_{10}(X)-\Upsilon_{10}(\bar{X})\|_G \preccurlyeq \beta_{D1}\|S_V-\bar{S}_V\|_G+m_V\|I_{V1}-\bar{I}_{V1}\|_G,$$

$$\|\Upsilon_{11}(X)-\Upsilon_{11}(\bar{X})\|_G \preccurlyeq \beta_{D2}\|S_V-\bar{S}_V\|_G+m_V\|I_{V2}-\bar{I}_{V2}\|_G.$$

Transforming the equations above into matrix form yields:

$$\begin{pmatrix} \|\Upsilon_1(X)-\Upsilon_1(\bar{X})\|_\infty \\ \|\Upsilon_2(X)-\Upsilon_2(\bar{X})\|_\infty \\ \|\Upsilon_3(X)-\Upsilon_3(\bar{X})\|_\infty \\ \|\Upsilon_4(X)-\Upsilon_4(\bar{X})\|_\infty \\ \|\Upsilon_5(X)-\Upsilon_5(\bar{X})\|_\infty \\ \|\Upsilon_6(X)-\Upsilon_6(\bar{X})\|_\infty \\ \|\Upsilon_7(X)-\Upsilon_7(\bar{X})\|_\infty \\ \|\Upsilon_8(X)-\Upsilon_8(\bar{X})\|_\infty \\ \|\Upsilon_9(X)-\Upsilon_9(\bar{X})\|_\infty \\ \|\Upsilon_{10}(X)-\Upsilon_{10}(\bar{X})\|_\infty \\ \|\Upsilon_{11}(X)-\Upsilon_{11}(\bar{X})\|_\infty \end{pmatrix} \preccurlyeq \amalg \begin{pmatrix} \|S_H-\bar{S}_H\|_\infty \\ \|I_{D1}-\bar{I}_{D1}\|_\infty \\ \|I_{D2}-\bar{I}_{D2}\|_\infty \\ \|I_C-\bar{I}_C\|_\infty \\ \|I_{DC1}-\bar{I}_{DC1}\|_\infty \\ \|I_{DC2}-\bar{I}_{DC2}\|_\infty \\ \|R_D-\bar{R}_D\|_\infty \\ \|R_C-\bar{R}_C\|_\infty \\ \|S_V-\bar{S}_V\|_\infty \\ \|I_{V1}-\bar{I}_{V1}\|_\infty \\ \|I_{V2}-\bar{I}_{V2}\|_\infty \end{pmatrix},$$

where

$$\amalg = \begin{pmatrix} 1-m_H & 0 & 0 & 0 & 0 & 0 & \theta_D & \theta_C & 0 & 0 & 0 \\ \beta_{V1} & \begin{pmatrix}\varepsilon_C+\tau_{D1}\\ +d_{D1}+m_H\end{pmatrix} & 0 & 0 & \tau_C & 0 & 0 & 1 & 0 & 0 & 0 \\ \beta_{V2} & 0 & \begin{pmatrix}\varepsilon_C-\tau_{D1}\\ -d_{D1}-m_H\end{pmatrix} & 0 & 0 & \tau_C & 0 & 1 & 0 & 0 & 0 \\ \beta_C & 0 & 0 & \begin{pmatrix}\tau_C+d_C\\ +m_H\\ +\varepsilon_{v1}+\varepsilon_{v2}\end{pmatrix} & \tau_{D1} & \tau_{D2} & 1 & 0 & 0 & 0 & 0 \\ 0 & \begin{vmatrix}\varepsilon_C-\tau_{D1}\\ -d_{D1}-m_H\\ -\tau_C-d_C\end{vmatrix} & 0 & \varepsilon_{v1} & 1 & 0 & 0 & 0 & 0 & 0 & 0 \\ 0 & 0 & \begin{vmatrix}\varepsilon_C-\tau_{D2}\\ -d_{D2}-m_H\\ -\tau_C-d_C\end{vmatrix} & \varepsilon_{v2} & 0 & 1 & 0 & 0 & 0 & 0 & 0 \\ 0 & \tau_{D1} & \tau_{D2} & 0 & 0 & 0 & \begin{pmatrix}1-m_H\\ -\beta_{V2}-\theta_D\end{pmatrix} & 0 & 0 & 0 & 0 \\ 0 & 0 & 0 & \tau_C & 0 & 0 & m_H & \begin{pmatrix}1+\beta_{V1}\\ +\beta_{V2}+\theta_C\end{pmatrix} & 0 & 0 & 0 \\ 0 & 0 & 0 & 0 & 0 & 0 & 0 & 0 & 1-m_V & 0 & 0 \\ 0 & 0 & 0 & 0 & 0 & 0 & 0 & 0 & \beta_{D1} & m_V & 0 \\ 0 & 0 & 0 & 0 & 0 & 0 & 0 & 0 & \beta_{D2} & 0 & m_V \end{pmatrix}.$$

□

Theorem 4 Assuming that the matrix

$$\frac{k}{\Gamma(\zeta)}\amalg, \tag{18}$$

converges to O_{11}, the initial value problem has a unique solution given by (13) belongs in $\bar{B}(X_0,\ \Delta)$.

Proof. Further, we have for any $X,\ \bar{X} \in \bar{B}(X_0,\ \pi)$, and by using Lemma 4.

$$\begin{aligned} \|\mathfrak{N}(X)-\mathfrak{N}(\bar{X})\|_G &= \left\| \frac{1}{\Gamma(\zeta)} \sum_{i=1}^{\rho} \frac{\Gamma(\rho-i+\zeta)}{\Gamma(\rho-i+1)} \left(\Upsilon(X(i-1))-\Upsilon(\bar{X}(i-1))\right) \right\|_G \\ &\preccurlyeq \frac{1}{\Gamma(\zeta)} \sum_{i=1}^{\rho} \left| \frac{\Gamma(\rho-i+\zeta)}{\Gamma(\rho-i+1)} \right| \left\| \Upsilon(X)-\Upsilon(\bar{X}) \right\|_G \\ &\preccurlyeq \frac{k}{\Gamma(\zeta)} \amalg \|X-\bar{X}\|_G. \end{aligned}$$

The convergence of the matrix $\frac{k}{\Gamma(\zeta)}\amalg$ to zero implies that $\mathfrak{N}$ is a G-contraction. Therefore, based on Perov's fixed point Theorem 3, system (13) is guaranteed to have a unique solution in $\bar{B}(X_0,\ \pi)$. □

5.1 *Stability analysis of the model*

In this section, we provide a comprehensive stability analysis of the proposed fractional-order co-circulation model, establishing both Ulam-Hyers stability and Lyapunov stability properties.

5.2 *Ulam-Hyers stability*

Ulam-Hyers stability ensures that small perturbations in the model equations lead to bounded deviations in the solutions, which is crucial for the robustness of our epidemiological model.

Theorem 5 (Ulam-Hyers Stability) The fractional-order discrete system (13) is Ulam-Hyers stable. That is, there exists a constant $C > 0$ such that for every $\varepsilon > 0$ and for every function $X^*(t)$ satisfying

$$\|{}^{C}\Delta_a^{\zeta}X^*(t) - \Upsilon(t+\zeta-1,\ X^*(t+\zeta-1))\|_G \leq \varepsilon, \quad \forall t \in \mathbb{N}_a,$$

there exists a solution $X(t)$ of system (13) such that

$$\|X^*(t) - X(t)\|_G \leq C\varepsilon, \quad \forall t \in \mathbb{N}_a.$$

Proof. Consider the fractional-order system:

$${}^{C}\Delta_a^{\zeta}X(t) = \Upsilon(t+\zeta-1,\ X(t+\zeta-1)).$$

Let $X^*(t)$ be an approximate solution satisfying:

$$\|{}^{C}\Delta_a^{\zeta}X^*(t) - \Upsilon(t+\zeta-1,\ X^*(t+\zeta-1))\|_G \leq \varepsilon.$$

Define the perturbation $\delta(t) = {}^{C}\Delta_a^{\zeta}X^*(t) - \Upsilon(t+\zeta-1,\ X^*(t+\zeta-1))$, with $\|\delta(t)\|_G \leq \varepsilon$.
Using the fractional integral representation, we have:

$$X^*(t) = X^*(a) + \frac{1}{\Gamma(\zeta)}\sum_{\tau=a}^{t-\zeta}(t-\tau-1)^{\zeta-1}[\Upsilon(\tau+\zeta-1,\ X^*(\tau+\zeta-1)) + \delta(\tau)].$$

Let $X(t)$ be the exact solution of the system. Then:

$$\|X^*(t)-X(t)\|_G = \left\| \frac{1}{\Gamma(\zeta)} \sum_{\tau=a}^{t-\zeta} (t-\tau-1)^{\zeta-1} [\Upsilon(\tau+\zeta-1,\, X^*(\tau+\zeta-1)) - \Upsilon(\tau+\zeta-1,\, X(\tau+\zeta-1)) + \delta(\tau)] \right\|_G$$

$$\leq \frac{1}{\Gamma(\zeta)} \sum_{\tau=a}^{t-\zeta} (t-\tau-1)^{\zeta-1} \left[L\|X^*(\tau+\zeta-1) - X(\tau+\zeta-1)\|_G + \varepsilon \right],$$

where L is the Lipschitz constant from Lemma 4.

Applying the generalized Gronwall inequality for fractional difference equations, there exists a constant $C > 0$ such that:

$$\|X^*(t)-X(t)\|_G \leq C\varepsilon, \quad \forall t \in \mathbb{N}_a.$$

This completes the proof of Ulam-Hyers stability. □

5.3 *Lyapunov stability analysis*

We now establish the Lyapunov stability of the Disease-Free Equilibrium (DFE) and analyze the stability properties of the endemic equilibrium.

Theorem 6 (Lyapunov Stability of DFE) The Disease-Free Equilibrium Ξ_0 of system (13) is locally asymptotically stable when $R_0 < 1$ and unstable when $R_0 > 1$.

Proof. Consider the Lyapunov function candidate:

$$V(X) = \frac{1}{2} \sum_{i=1}^{11} (X_i - X_i^0)^2,$$

where $X = (S_H,\, I_{D1},\, I_{D2},\, I_C,\, I_{DC1},\, I_{DC2},\, R_D,\, R_C,\, S_V,\, I_{V1},\, I_{V2})$ and X^0 represents the DFE.

The Caputo fractional difference of V along the solutions of system (13) is:

$${}^C\Delta_a^{\zeta} V(X(t)) \leq \sum_{i=1}^{11} (X_i(t+\zeta-1) - X_i^0)\, {}^C\Delta_a^{\zeta} X_i(t).$$

Substituting the system equations and evaluating at the DFE, we obtain:

$$\begin{aligned} {}^C\Delta_a^{\zeta} V(X(t)) \leq & - m_H (S_H - S_H^0)^2 - m_V (S_V - S_V^0)^2 \\ & + (R_0 - 1) \left[\beta_{V1} I_{V1} + \beta_{V2} I_{V2} + \beta_C (I_C + I_{DC1} + I_{DC2}) \right] \\ & - \sum_{i \in \mathscr{I}} \alpha_i X_i^2 + \text{higer order terms}, \end{aligned}$$

where $\mathscr{I}$ represents the infected compartments and $\alpha_i > 0$ are positive constants.

When $R_0 < 1$, we have ${}^{C}\Delta_a^{\zeta} V(X(t)) < 0$ for all $X \neq X^0$ in a neighborhood of the DFE, establishing local asymptotic stability.

When $R_0 > 1$, the DFE becomes unstable due to the positive terms arising from infection dynamics. □

Theorem 7 (Global Stability of DFE) When $R_0 < 1$, the disease-free equilibrium Ξ_0 is globally asymptotically stable in the biologically feasible region Ω.

Proof. Consider the Lyapunov function:

$$L(t) = \sum_{i \in \mathscr{I}} c_i X_i(t),$$

where $\mathscr{I}$ represents all infected compartments and $c_i > 0$ are carefully chosen positive constants.

The fractional difference of L satisfies:

$${}^{C}\Delta_a^{\zeta} L(t) \leq (R_0 - 1)K - \mu L(t),$$

where $K > 0$ and $\mu > 0$ are constants.

When $R_0 < 1$, we have ${}^{C}\Delta_a^{\zeta} L(t) \leq -\mu L(t)$, which implies $L(t) \to 0$ as $t \to \infty$. Consequently, all infected compartments approach zero, and the system converges to the DFE. □

Theorem 8 (Stability of Endemic Equilibrium) When $R_0 > 1$, the endemic equilibrium Ξ^* is locally asymptotically stable under appropriate parameter conditions.

Proof. The Jacobian matrix $J(\Xi^*)$ evaluated at the endemic equilibrium has characteristic equation:

$$\det(\lambda I - J(\Xi^*)) = 0.$$

Using the fractional Routh-Hurwitz criteria and the properties of Metzler matrices, we can show that all eigenvalues satisfy $|\arg(\lambda)| > \dfrac{\zeta\pi}{2}$ when the following conditions hold:

1. The transmission rates satisfy certain boundedness conditions.
2. The recovery rates are sufficiently large compared to transmission rates.
3. The cross-immunity parameters maintain system cooperativity.

These conditions ensure the local asymptotic stability of the endemic equilibrium. □

5.4 *Numerical verification of stability*

Proposition 4 The numerical simulations in section 7 confirm the theoretical stability results:

• For $R_0 < 1$, solutions converge to the DFE.

• For $R_0 > 1$, solutions approach the endemic equilibrium.

• The system exhibits robust behavior under small perturbations.

6. Crossover discrete time model analysis and numerical schemes

Crossover models in discrete systems offer a powerful framework for capturing complex epidemic dynamics. By combining different operators, such as fractional and variable-order derivatives, they allow for modeling varying disease behaviors across different time intervals. This approach enhances accuracy by reflecting real-world changes in transmission

or control strategies while also uncovering rich dynamics like oscillations or bifurcations. Additionally, crossover models provide improved insights into the timing and effectiveness of interventions, making them valuable for informed decision-making during epidemic control.

In this part, we will introduce two novel crossover discrete-time systems. In the first crossover discrete-time system, we will define the fractional discrete model (12) in the interval of time $t_0 < t \leq t_1$, and the variable order discrete model (14) in the interval of time $t_1 < t \leq T_f$.

In the second crossover discrete-time system, we will define the variable order discrete model (12) in the interval of time $t_0 < t \leq t_1$, and the fractional discrete model (14) in the interval of time $t_1 < t \leq T_f$.

According to Theorem 1, the numerical formula of the fractional discrete-time of the two strains of COVID-19 and dengue co-circulating epidemic model (12) is designed as:

$$S_H(t_{\rho_1}) = S_H(0) + \frac{1}{\Gamma(\zeta)} \sum_{\tau=a+\rho_1-\zeta}^{\rho_1-\zeta} (\rho_1 - \tau - 1)^{\zeta-1} \Upsilon_1(\tau - 1 + \zeta,\ \vartheta(\tau - 1 + \zeta)),$$

$$I_{D1}(t_{\rho_1}) = I_{D1}(0) + \frac{1}{\Gamma(\zeta)} \sum_{\tau=a+\rho_1-\zeta}^{\rho_1-\zeta} (\rho - \tau - 1)^{\zeta-1} \Upsilon_2(\tau - 1 + \zeta,\ \vartheta(\tau - 1 + \zeta)),$$

$$I_{D2}(t_{\rho_1}) = I_{D2}(0) + \frac{1}{\Gamma(\zeta)} \sum_{\tau=a+\rho_1-\zeta}^{\rho_1-\zeta} (\rho_1 - \tau - 1)^{\zeta-1} \Upsilon_3(\tau - 1 + \zeta,\ \vartheta(\tau - 1 + \zeta)),$$

$$I_C(t_{\rho_1}) = I_C(0) + \frac{1}{\Gamma(\zeta)} \sum_{\tau=a+\rho_1-\zeta}^{\rho_1-\zeta} (\rho_1 - \tau - 1)^{\zeta-1} \Upsilon_4(\tau - 1 + \zeta,\ \vartheta(\tau - 1 + \zeta)),$$

$$I_{DC1}(t_{\rho_1}) = I_{DC1}(0) + \frac{1}{\Gamma(\zeta)} \sum_{\tau=a+\rho_1-\zeta}^{\rho_1-\zeta} (\rho_1 - \tau - 1)^{\zeta-1} \Upsilon_5(\tau - 1 + \zeta,\ \vartheta(\tau - 1 + \zeta)),$$

$$I_{DC2}(t_{\rho_1}) = I_{DC2}(0) + \frac{1}{\Gamma(\zeta)} \sum_{\tau=a+\rho_1-\zeta}^{\rho_1-\zeta} (\rho_1 - \tau - 1)^{\zeta-1} \Upsilon_6(\tau - 1 + \zeta,\ \vartheta(\tau - 1 + \zeta)),$$

$$R_D(t_{\rho_1}) = R_D(0) + \frac{1}{\Gamma(\zeta)} \sum_{\tau=a+\rho_1-\zeta}^{\rho_1-\zeta} (\rho_1 - \tau - 1)^{\zeta-1} \Upsilon_7(\tau - 1 + \zeta,\ \vartheta(\tau - 1 + \zeta)),$$

$$R_C(t_{\rho_1}) = R_C(0) + \frac{1}{\Gamma(\zeta)} \sum_{\tau=a+\rho_1-\zeta}^{\rho_1-\zeta} (\rho_1 - \tau - 1)^{\zeta-1} \Upsilon_8(\tau - 1 + \zeta,\ \vartheta(\tau - 1 + \zeta)),$$

$$S_V(t_{\rho_1}) = S_V(0) + \frac{1}{\Gamma(\zeta)} \sum_{\tau=a+\rho_1-\zeta}^{\rho_1-\zeta} (\rho_1 - \tau - 1)^{\zeta-1} \Upsilon_9(\tau - 1 + \zeta,\ \vartheta(\tau - 1 + \zeta)),$$

$$I_{V1}(t_{\rho_1}) = I_{V1}(0) + \frac{1}{\Gamma(\zeta)} \sum_{\tau=a+\rho_1-\zeta}^{\rho_1-\zeta} (\rho_1 - \tau - 1)^{\zeta-1} \Upsilon_{10}(\tau - 1 + \zeta,\ \vartheta(\tau - 1 + \zeta)),$$

$$I_{V2}(t_{\rho_1}) = I_{V2}(0) + \frac{1}{\Gamma(\zeta)} \sum_{\tau=a+\rho_1-\zeta}^{\rho_1-\zeta} (\rho_1 - \tau - 1)^{\zeta-1} \Upsilon_{11}(\tau - 1 + \zeta,\ \vartheta(\tau - 1 + \zeta)), \tag{19}$$

where

$$\vartheta(\tau+\zeta-1) = \Big\{ S_H(\tau+\zeta-1),\ I_{D1}(\tau+\zeta-1),\ I_{D2}(\tau+\zeta-1),\ I_C(\tau+\zeta-1),\ I_{DC1}(\tau+\zeta-1),$$

$$I_{DC2}(\tau+\zeta-1),\ R_D(\tau+\zeta-1),\ R_C(\tau+\zeta-1),\ S_V(\tau+\zeta-1),\ I_{V1}(\tau+\zeta-1),\ I_{V2}(\tau+\zeta-1) \Big\}.$$

Setting $a = 0$ and recognizing that $(\rho_1 - \tau - 1)^{\zeta-1} = \dfrac{\Gamma(\rho_1 - \tau)}{\Gamma(\rho_1 - \tau - \zeta + 1)}$, we can derive the numerical formula for (19) from Theorem 1, as shown in [33].

$$S_H(t_{\rho_1}) = S_H(0) + \frac{1}{\Gamma(\zeta)} \sum_{i=1}^{\rho_1} \frac{\Gamma(\rho_1 - i + \zeta)}{\Gamma(\rho_1 - i + 1)} \Upsilon_1(i-1,\ \vartheta(i-1)),$$

$$I_{D1}(t_{\rho_1}) = I_{D1}(0) + \frac{1}{\Gamma(\zeta)} \sum_{i=1}^{\rho_1} \frac{\Gamma(\rho_1 - i + \zeta)}{\Gamma(\rho_1 - i + 1)} \Upsilon_2(i-1,\ \vartheta(i-1)),$$

$$I_{D2}(t_{\rho_1}) = I_{D2}(0) + \frac{1}{\Gamma(\zeta)} \sum_{i=1}^{\rho_1} \frac{\Gamma(\rho_1 - i + \zeta)}{\Gamma(\rho_1 - i + 1)} \Upsilon_3(i-1,\ \vartheta(i-1)),$$

$$I_C(t_{\rho_1}) = I_C(0) + \frac{1}{\Gamma(\zeta)} \sum_{i=1}^{\rho_1} \frac{\Gamma(\rho_1 - i + \zeta)}{\Gamma(\rho - i + 1)} \Upsilon_4(i-1,\ \vartheta(i-1)),$$

$$I_{DC1}(t_{\rho_1}) = I_{DC1}(0) + \frac{1}{\Gamma(\zeta)} \sum_{i=1}^{\rho_1} \frac{\Gamma(\rho_1 - i + \zeta)}{\Gamma(\rho_1 - i + 1)} \Upsilon_5(i-1,\ \vartheta(i-1)),$$

$$I_{DC2}(t_{\rho_1}) = I_{DC2}(0) + \frac{1}{\Gamma(\zeta)} \sum_{i=1}^{\rho_1} \frac{\Gamma(\rho_1 - i + \zeta)}{\Gamma(\rho_1 - i + 1)} \Upsilon_6(i-1,\ \vartheta(i-1)),$$

$$R_D(t_{\rho_1}) = R_D(0) + \frac{1}{\Gamma(\zeta)} \sum_{i=1}^{\rho_1} \frac{\Gamma(\rho_1 - i + \zeta)}{\Gamma(\rho_1 - i + 1)} \Upsilon_7(i-1,\ \vartheta(i-1)),$$

$$R_C(t_{\rho_1}) = R_C(0) + \frac{1}{\Gamma(\zeta)} \sum_{i=1}^{\rho_1} \frac{\Gamma(\rho_1 - i + \zeta)}{\Gamma(\rho - i + 1)} \Upsilon_8(i-1,\ \vartheta(i-1)),$$

$$S_V(t_{\rho_1}) = S_V(0) + \frac{1}{\Gamma(\zeta)} \sum_{i=1}^{\rho_1} \frac{\Gamma(\rho_1 - i + \zeta)}{\Gamma(\rho_1 - i + 1)} \Upsilon_9(i-1,\ \vartheta(i-1)),$$

$$I_{V1}(t_{\rho_1}) = I_{V1}(0) + \frac{1}{\Gamma(\zeta)} \sum_{i=1}^{\rho_1} \frac{\Gamma(\rho_1 - i + \zeta)}{\Gamma(\rho_1 - i + 1)} \Upsilon_{10}(i-1,\ \vartheta(i-1)),$$

$$I_{V2}(t_{\rho_1}) = I_{V2}(0) + \frac{1}{\Gamma(\zeta)} \sum_{i=1}^{\rho_1} \frac{\Gamma(\rho_1 - i + \zeta)}{\Gamma(\rho_1 - i + 1)} \Upsilon_{11}(i-1,\ \vartheta(i-1)), \tag{20}$$

where

$$\vartheta(i-1) = \Big\{ S_H(i-1),\ I_{D1}(i-1),\ I_{D2}(i-1),\ I_C(i-1),\ I_{DC1}(i-1),$$

$$I_{DC2}(i-1),\ R_D(i-1),\ R_C(i-1),\ S_V(i-1),\ I_{V1}(i-1),\ I_{V2}(i-1) \Big\}.$$

Now, to solve the first crossover model (12) in the interval of time $t_0 < t \leq t_1$, and the variable order discrete model (14) in the interval of time $t_1 < t \leq T_f$. In the first interval, we will use the scheme (20) and the following scheme to solve the model in the second interval of time $t_1 < t \leq T_f$:

$$S_H(t_\rho) = S_H(0) + \frac{1}{\Gamma(\zeta(t_\rho))} \sum_{i=\rho_1}^{\rho} \frac{\Gamma(\rho - i + \zeta(t_\rho))}{\Gamma(\rho - i + 1)} \Upsilon_1(i-1,\ \vartheta(i-1)),$$

$$I_{D1}(t_\rho) = I_{D1}(0) + \frac{1}{\Gamma(\zeta(t_\rho))} \sum_{i=\rho_1}^{\rho} \frac{\Gamma(\rho - i + \zeta(t_\rho))}{\Gamma(\rho - i + 1)} \Upsilon_2(i-1,\ \vartheta(i-1)),$$

$$I_{D2}(t_\rho) = I_{D2}(0) + \frac{1}{\Gamma(\zeta(t_\rho))} \sum_{i=\rho_1}^{\rho} \frac{\Gamma(\rho - i + \zeta(t_\rho))}{\Gamma(\rho - i + 1)} \Upsilon_3(i-1,\ \vartheta(i-1)),$$

$$I_C(t_\rho) = I_C(0) + \frac{1}{\Gamma(\zeta(t_\rho))} \sum_{i=\rho_1}^{\rho} \frac{\Gamma(\rho - i + \zeta(t_\rho))}{\Gamma(\rho - i + 1)} \Upsilon_4(i-1,\ \vartheta(i-1)),$$

$$I_{DC1}(t_\rho) = I_{DC1}(0) + \frac{1}{\Gamma(\zeta(t_\rho))} \sum_{i=\rho_1}^{\rho} \frac{\Gamma(\rho - i + \zeta(t_\rho))}{\Gamma(\rho - i + 1)} \Upsilon_5(i-1,\ \vartheta(i-1)),$$

$$I_{DC2}(t_\rho) = I_{DC2}(0) + \frac{1}{\Gamma(\zeta(t_\rho))} \sum_{i=\rho_1}^{\rho} \frac{\Gamma(\rho - i + \zeta(t_\rho))}{\Gamma(\rho - i + 1)} \Upsilon_6(i-1,\ \vartheta(i-1)),$$

$$R_D(t_\rho) = R_D(0) + \frac{1}{\Gamma(\zeta(t_\rho))} \sum_{i=\rho_1}^{\rho} \frac{\Gamma(\rho - i + \zeta(t_\rho))}{\Gamma(\rho - i + 1)} \Upsilon_7(i-1,\ \vartheta(i-1)),$$

$$R_C(t_\rho) = R_C(0) + \frac{1}{\Gamma(\zeta(t_\rho))} \sum_{i=\rho_1}^{\rho} \frac{\Gamma(\rho - i + \zeta(t_\rho))}{\Gamma(\rho - i + 1)} \Upsilon_8(i-1,\ \vartheta(i-1)),$$

$$S_V(t_\rho) = S_V(0) + \frac{1}{\Gamma(\zeta(t_\rho))} \sum_{i=\rho_1}^{\rho} \frac{\Gamma(\rho - i + \zeta(t_\rho))}{\Gamma(\rho - i + 1)} \Upsilon_9(i-1,\ \vartheta(i-1)),$$

$$I_{V1}(t_\rho) = I_{V1}(0) + \frac{1}{\Gamma(\zeta(t_\rho))} \sum_{i=\rho_1}^{\rho} \frac{\Gamma(\rho - i + \zeta(t_\rho))}{\Gamma(\rho - i + 1)} \Upsilon_{10}(i-1,\ \vartheta(i-1)),$$

$$I_{V2}(t_\rho) = I_{V2}(0) + \frac{1}{\Gamma(\zeta(t_\rho))} \sum_{i=\rho_1}^{\rho} \frac{\Gamma(\rho - i + \zeta(t_\rho))}{\Gamma(\rho - i + 1)} \Upsilon_{11}(i-1,\ \vartheta(i-1)) \tag{21}$$

To solve the second crossover model; the variable order discrete model (14) in the interval of time $t_0 < t \leq t_1$, and the fractional order discrete model (12) in the interval of time $t_1 < t \leq T_f$. In the first interval we will use the following scheme:

$$S_H(t_{\rho_1}) = S_H(0) + \frac{1}{\Gamma(\zeta(t_{\rho_1}))} \sum_{i=1}^{\rho_1} \frac{\Gamma(\rho_1 - i + \zeta(t_{\rho_1}))}{\Gamma(\rho_1 - i + 1)} \Upsilon_1(i-1,\ \vartheta(i-1)),$$

$$I_{D1}(t_{\rho_1}) = I_{D1}(0) + \frac{1}{\Gamma(\zeta(t_{\rho_1}))} \sum_{i=1}^{\rho_1} \frac{\Gamma(\rho_1 - i + \zeta(t_{\rho_1}))}{\Gamma(\rho_1 - i + 1)} \Upsilon_2(i-1,\ \vartheta(i-1)),$$

$$I_{D2}(t_{\rho_1}) = I_{D2}(0) + \frac{1}{\Gamma(\zeta(t_{\rho_1}))} \sum_{i=1}^{\rho_1} \frac{\Gamma(\rho_1 - i + \zeta(t_{\rho_1}))}{\Gamma(\rho_1 - i + 1)} \Upsilon_3(i-1,\ \vartheta(i-1)),$$

$$I_C(t_{\rho_1}) = I_C(0) + \frac{1}{\Gamma(\zeta(\rho))} \sum_{i=1}^{\rho_1} \frac{\Gamma(\rho_1 - i + \zeta(t_{\rho_1}))}{\Gamma(\rho_1 - i + 1)} \Upsilon_4(i-1,\ \vartheta(i-1)),$$

$$I_{DC1}(t_{\rho_1}) = I_{DC1}(0) + \frac{1}{\Gamma(\zeta(t_{\rho_1}))} \sum_{i=1}^{\rho_1} \frac{\Gamma(\rho_1 - i + \zeta(t_{\rho_1}))}{\Gamma(\rho_1 - i + 1)} \Upsilon_5(i-1,\ \vartheta(i-1)),$$

$$I_{DC2}(t_{\rho_1}) = I_{DC2}(0) + \frac{1}{\Gamma(\zeta(t_{\rho_1}))} \sum_{i=1}^{\rho_1} \frac{\Gamma(\rho - i + \zeta(t_{\rho_1}))}{\Gamma(\rho_1 - i + 1)} \Upsilon_6(i-1,\ \vartheta(i-1)),$$

$$R_D(t_{\rho_1}) = R_D(0) + \frac{1}{\Gamma(\zeta(t_{\rho_1}))}\sum_{i=1}^{\rho_1}\frac{\Gamma(\rho_1 - i + \zeta(t_{\rho_1}))}{\Gamma(\rho_1 - i + 1)}\Upsilon_7(i-1,\ \vartheta(i-1)),$$

$$R_C(t_{\rho_1}) = R_C(0) + \frac{1}{\Gamma(\zeta(t_{\rho_1}))}\sum_{i=1}^{\rho_1}\frac{\Gamma(\rho_1 - i + \zeta(t_{\rho_1}))}{\Gamma(\rho_1 - i + 1)}\Upsilon_8(i-1,\ \vartheta(i-1)),$$

$$S_V(t_{\rho_1}) = S_V(0) + \frac{1}{\Gamma(\zeta(\rho_1))}\sum_{i=1}^{\rho_1}\frac{\Gamma(\rho_1 - i + \zeta(t_{\rho_1}))}{\Gamma(\rho_1 - i + 1)}\Upsilon_9(i-1,\ \vartheta(i-1)),$$

$$I_{V1}(t_{\rho_1}) = I_{V1}(0) + \frac{1}{\Gamma(\zeta(t_{\rho_1}))}\sum_{i=1}^{\rho_1}\frac{\Gamma(\rho_1 - i + \zeta(t_{\rho_1}))}{\Gamma(\rho_1 - i + 1)}\Upsilon_{10}(i-1,\ \vartheta(i-1)),$$

$$I_{V2}(t_{\rho_1}) = I_{V2}(0) + \frac{1}{\Gamma(\zeta(\rho))}\sum_{i=1}^{\rho_1}\frac{\Gamma(\rho_1 - i + \zeta(t_{\rho_1}))}{\Gamma(\rho_1 - i + 1)}\Upsilon_{11}(i-1,\ \vartheta(i-1)), \tag{22}$$

and the following scheme to solve the second crossover model in the second interval of time $\rho_1 < \rho \leq T_f$:

$$S_H(t_\rho) = S_H(0) + \frac{1}{\Gamma(\zeta)}\sum_{i=\rho_1}^{\rho}\frac{\Gamma(\rho - i + \zeta)}{\Gamma(\rho - i + 1)}\Upsilon_1(i-1,\ \vartheta(i-1)),$$

$$I_{D1}(t_\rho) = \frac{1}{\Gamma(\zeta)}\sum_{i=\rho_1}^{\rho}\Upsilon_2(i-1,\ \vartheta(i-1))\frac{\Gamma(\rho - \zeta + i)}{\Gamma(\rho + 1 - i)} + I_{D1}(0),$$

$$I_{D2}(t_\rho) = \frac{1}{\Gamma(\zeta)}\sum_{i=\rho_1}^{\rho}\Upsilon_3(i-1,\ \vartheta(i-1))\frac{\Gamma(\rho + \zeta - i)}{\Gamma(1 + \rho - i)} + I_{D2}(0),$$

$$I_C(t_\rho) = I_C(0) + \frac{1}{\Gamma(\zeta)}\sum_{i=\rho_1}^{\rho}\frac{\Gamma(\rho - i + \zeta)}{\Gamma(\rho - i + 1)}\Upsilon_4(i-1,\ \vartheta(i-1)),$$

$$I_{DC1}(t_\rho) = I_{DC1}(0) + \frac{1}{\Gamma(\zeta)}\sum_{i=\rho_1}^{\rho}\frac{\Gamma(\rho - i + \zeta)}{\Gamma(\rho - i + 1)}\Upsilon_5(i-1,\ \vartheta(i-1)),$$

$$I_{DC2}(t_\rho) = \frac{1}{\Gamma(\zeta)}\sum_{i=\rho_1}^{\rho}\Upsilon_6(i-1,\ \vartheta(i-1))\frac{\Gamma(\rho + \zeta - i)}{\Gamma(\rho + 1 - i)} + I_{DC2}(0),$$

$$R_D(t_\rho) = R_D(0) + \frac{1}{\Gamma(\zeta)}\sum_{i=\rho_1}^{\rho}\frac{\Gamma(\rho - i + \zeta)}{\Gamma(\rho - i + 1)}\Upsilon_7(i-1,\ \vartheta(i-1)),$$

$$R_C(t_\rho) = R_C(0) + \frac{1}{\Gamma(\zeta)} \sum_{i=\rho_1}^{\rho} \frac{\Gamma(\rho - i + \zeta)}{\Gamma(\rho - i + 1)} \Upsilon_8(i-1,\ \vartheta(i-1)),$$

$$S_V(t_\rho) = S_V(0) + \frac{1}{\Gamma(\zeta)} \sum_{i=\rho_1}^{\rho} \frac{\Gamma(\rho - i + \zeta)}{\Gamma(\rho - i + 1)} \Upsilon_9(i-1,\ \vartheta(i-1)),$$

$$I_{V1}(t_\rho) = I_{V1}(0) + \frac{1}{\Gamma(\zeta)} \sum_{i=\rho_1}^{\rho} \frac{\Gamma(\rho - i + \zeta)}{\Gamma(\rho - i + 1)} \Upsilon_{10}(i-1,\ \vartheta(i-1)),$$

$$I_{V2}(t_\rho) = I_{V2}(0) + \frac{1}{\Gamma(\zeta)} \sum_{i=\rho_1}^{\rho} \Upsilon_{11}(i-1,\ \vartheta(i-1)) \frac{\Gamma(\rho + \zeta - i)}{\Gamma(1 + \rho - i)}. \tag{23}$$

7. Results and discussion

This section presents the numerical simulation of the proposed crossover epidemiological models. Specifically, we analyze the behavior of the first crossover model denoted by system (12) on the interval $t_0 < t \leq t_1$, followed by system (14) on $t_1 < t \leq T_f$ as well as the second crossover model, which follows the same structure. The initial conditions used in the simulation are: $S_H(0) = 3{,}600{,}000$, $I_{D1}(0) = 145$, $I_{D2}(0) = 146$, $I_C(0) = 247{,}534$, $I_{DC1}(0) = I_{DC2}(0) = R_D(0) = R_C(0) = 0$, and for vectors, $S_V(0) = 100{,}000$, $I_{V1}(0) = I_{V2}(0) = 5000$.

The demographic data employed for the simulations are based on Amazonas State, Brazil, with an estimated population of 4,269,995 and an average life expectancy of 74.90 years [38]. These values yield a daily recruitment rate of $\Lambda_H = \frac{4{,}269{,}995}{74.90 \times 365}$ and a natural human mortality rate of $m_H = \frac{1}{74.90 \times 365}$. All model parameters are specified in Table 2.

The computations were conducted using MATLAB R2021b on a system with an Intel(R) Core i5-3110M CPU @ 1.80 GHz and 8 GB RAM. To solve the systems, we applied the numerical schemes described in (20) and (21) for the first crossover model, and (23) and (22) for the second.

Figures 3 and 4 illustrate the behavior of the first crossover model (12)–(14) under different fractional-order parameters ζ and variable-order functions $\zeta(t)$, with $t_0 = 0$, $t_1 = 10$, and $T_f = 100$. The 3D plot in Figure 3 displays solution profiles for constant $\zeta = 0.85$ and time-varying $\zeta(t) = 0.90 - 0.001t$, while 2D projections in Figures 4 show the sensitivity of the solution to different fractional orders before and after the crossover point. Prior to t_1, the system exhibits multiple dynamic behaviors, whereas after t_1, the impact of fractional order on the dynamics significantly attenuates.

Biological interpretations of the vector dynamics under varying ζ values are as follows:

• Susceptible Vectors (S_V): The susceptible population steadily declines due to ongoing infection. Lower ζ values slow this decline, reflecting the memory effect of fractional dynamics, which biologically mimics delays in transmission.

• Vectors Infected with Dengue Strain 1 (I_{V1}): The infected population initially rises and then declines due to death or recovery. Slower decay for lower ζ reflects latent infection stages or delayed vector responses.

• Vectors Infected with Dengue Strain 2 (I_{V2}): The dynamics mirror those of I_{V1}, with differences in decay rate attributed to the same memory-based delays and potential inter-strain competition.

Figures 5–7 further explore the second crossover model. Figure 5 shows interrelations among infected and recovered populations for dengue and COVID-19 strains. It highlights the increase in recoveries and decline in infections, particularly post t_1, where the dynamic behavior changes significantly. This shift suggests that fractional memory effects predominantly influence early dynamics.

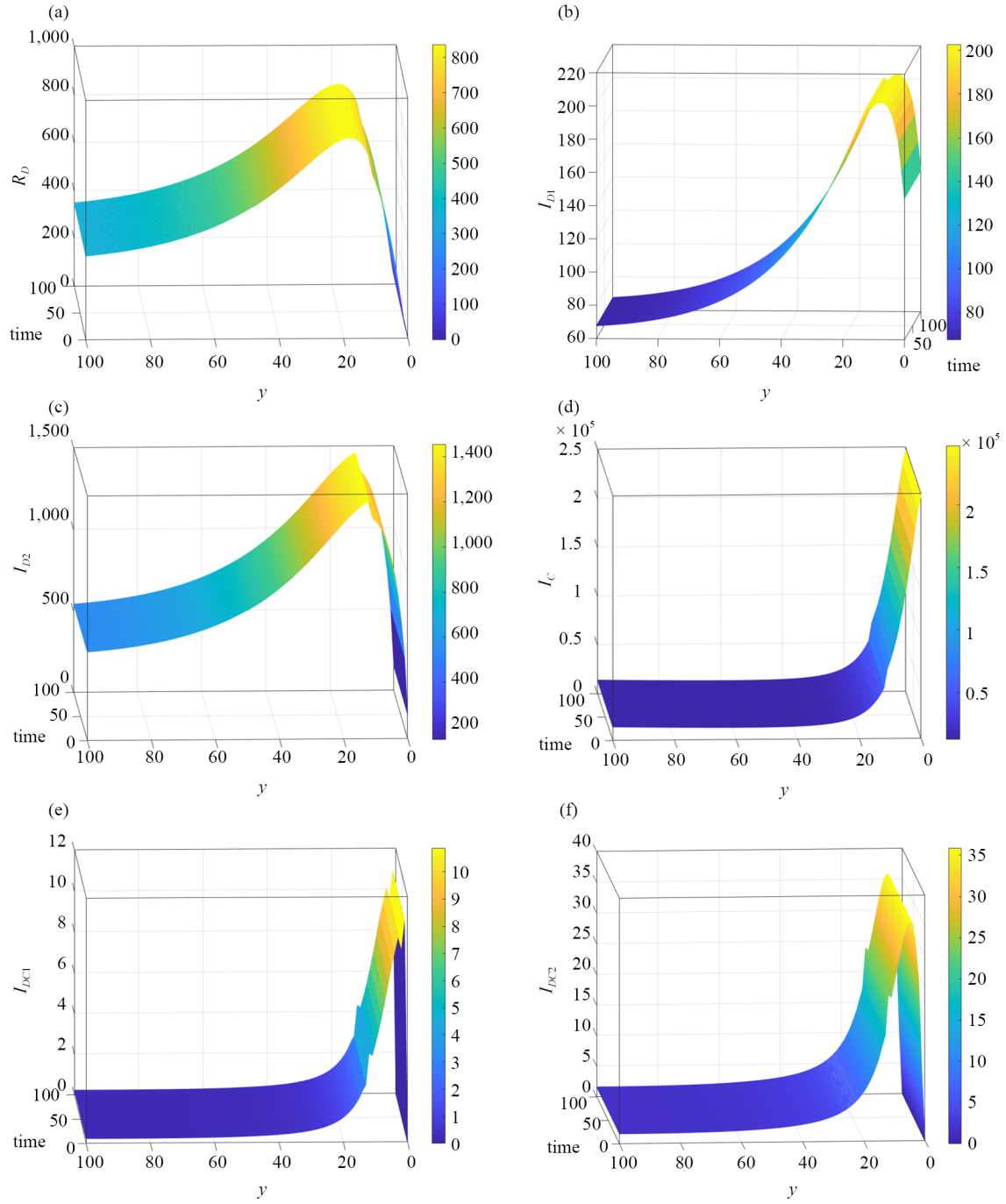

Figure 3. Simulation for first crossover model (12) and (14) with $\zeta = 0.85$ and $\zeta(t) = 0.90 - 0.001t$

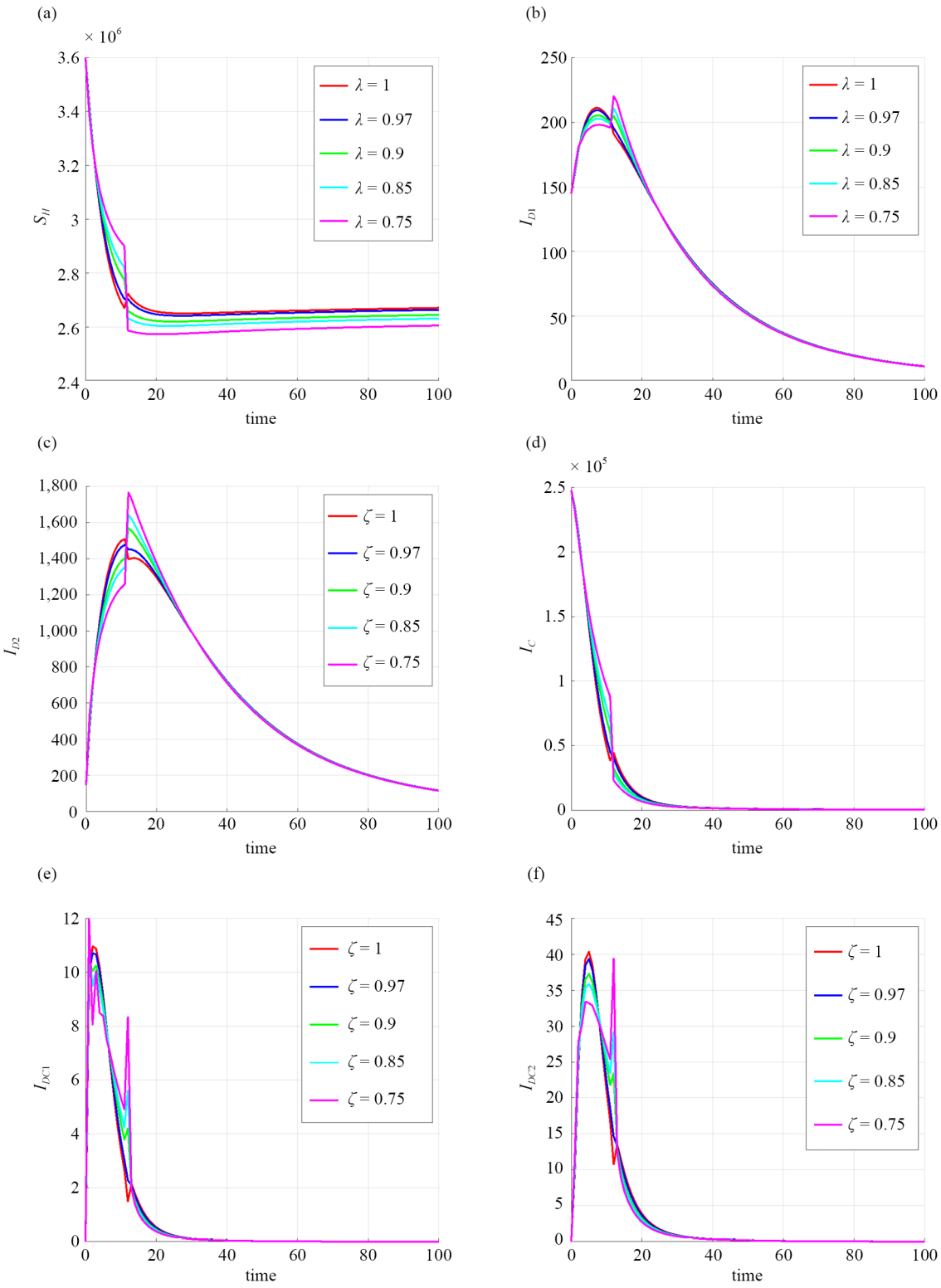
(a)
× 10^6
3.6
3.4
3.2
3
2.8
2.6
2.4
S_H
0
20
40
60
80
100
time
λ = 1
λ = 0.97
λ = 0.9
λ = 0.85
λ = 0.75
(b)
250
200
150
100
50
0
I_D1
time
(c)
1,800
1,600
1,400
1,200
1,000
800
600
400
200
0
I_D2
time
ζ = 1
ζ = 0.97
ζ = 0.9
ζ = 0.85
ζ = 0.75
(d)
× 10^5
2.5
2
1.5
1
0.5
0
I_C
time
(e)
12
10
8
6
4
2
0
I_DC1
time
(f)
45
40
35
30
25
20
15
10
5
0
I_DC2
time

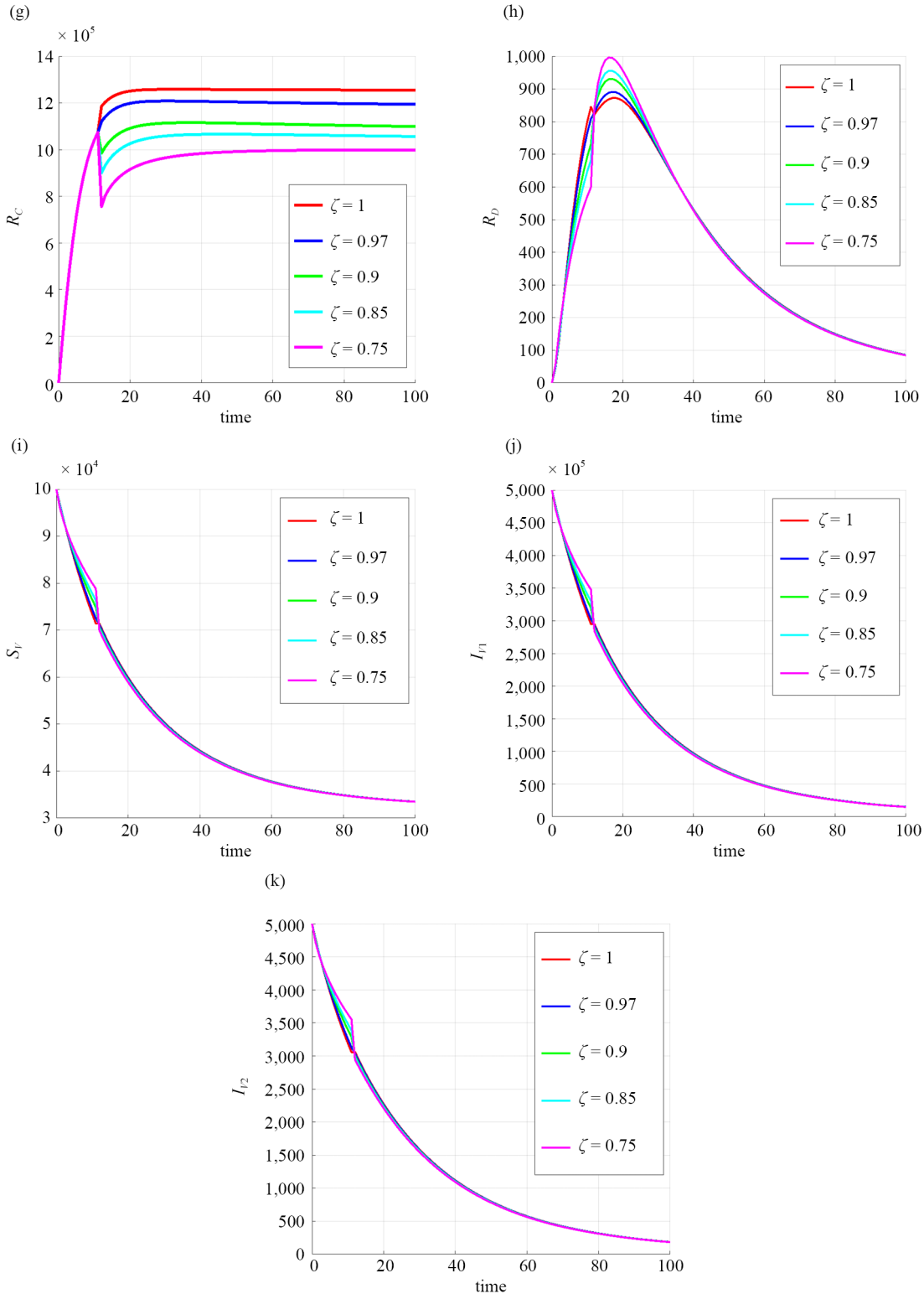

Figure 4. Simulation for first crossover model (12) and (14) with different ζ and $\zeta(t) = 0.96 - 0.0001(\sin(t/10))^2$

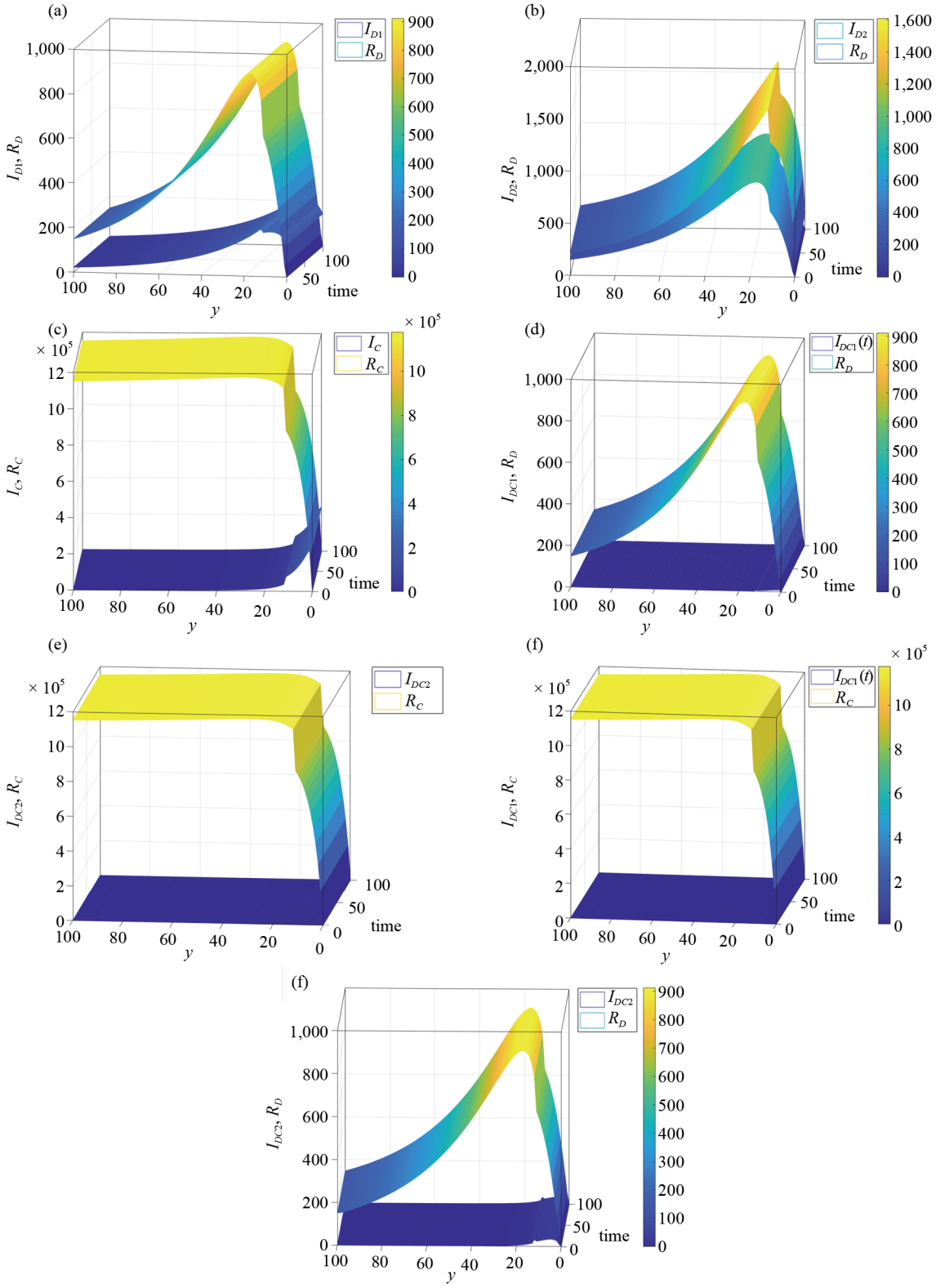

Figure 5. Simulation for second crossover model (14) and (12) with $\zeta = 0.92$ and $\zeta(t) = 0.80 - 0.001t$

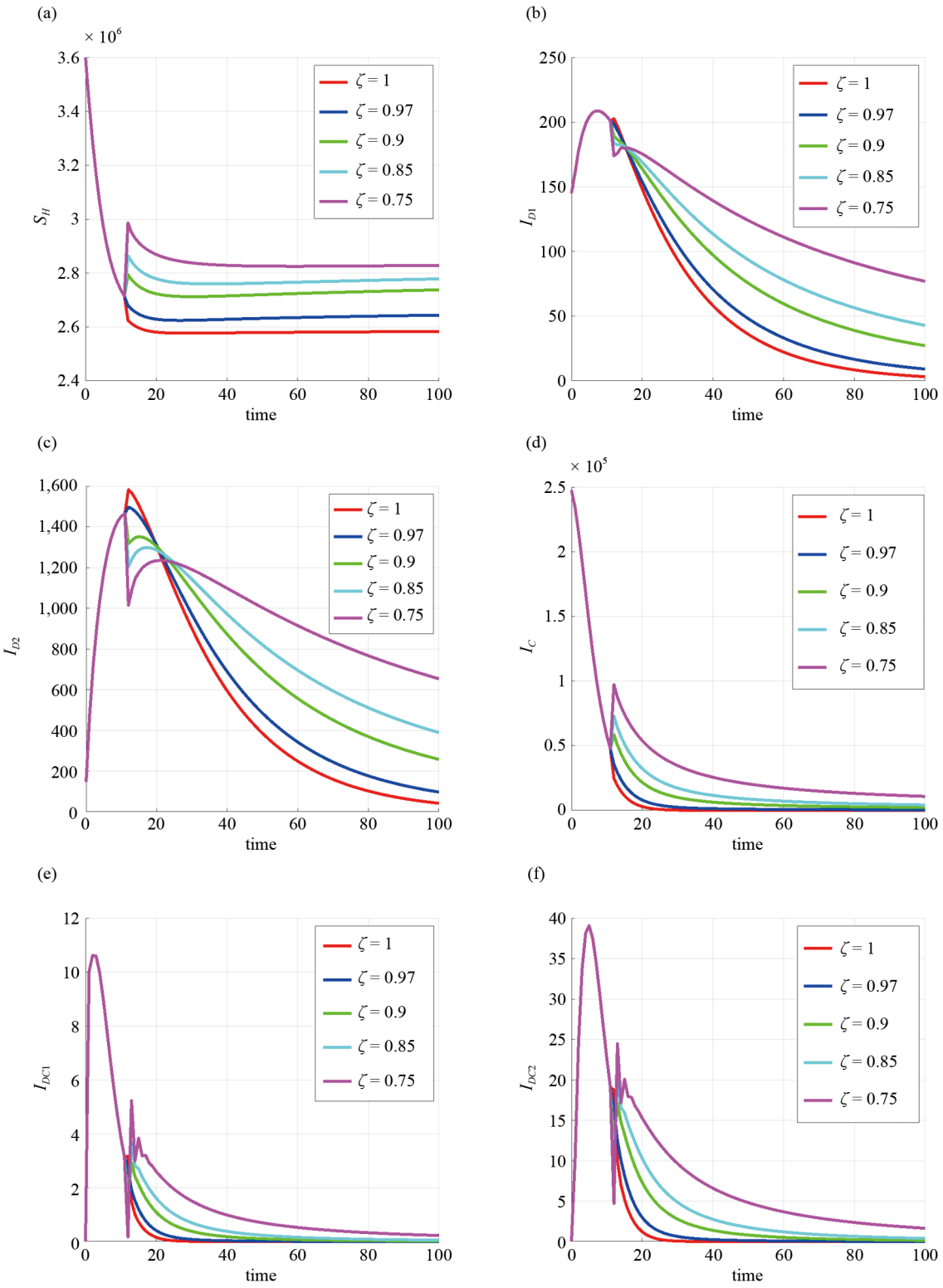
(a)
× 10^6
3.6
3.4
3.2
3
2.8
2.6
2.4
S_H
0
20
40
60
80
100
time
ζ = 1
ζ = 0.97
ζ = 0.9
ζ = 0.85
ζ = 0.75
(b)
250
200
150
100
50
0
I_D1
time
(c)
1,600
1,400
1,200
1,000
800
600
400
200
0
I_D2
time
(d)
× 10^5
2.5
2
1.5
1
0.5
0
I_C
time
(e)
12
10
8
6
4
2
0
I_DC1
time
(f)
40
35
30
25
20
15
10
5
0
I_DC2
time

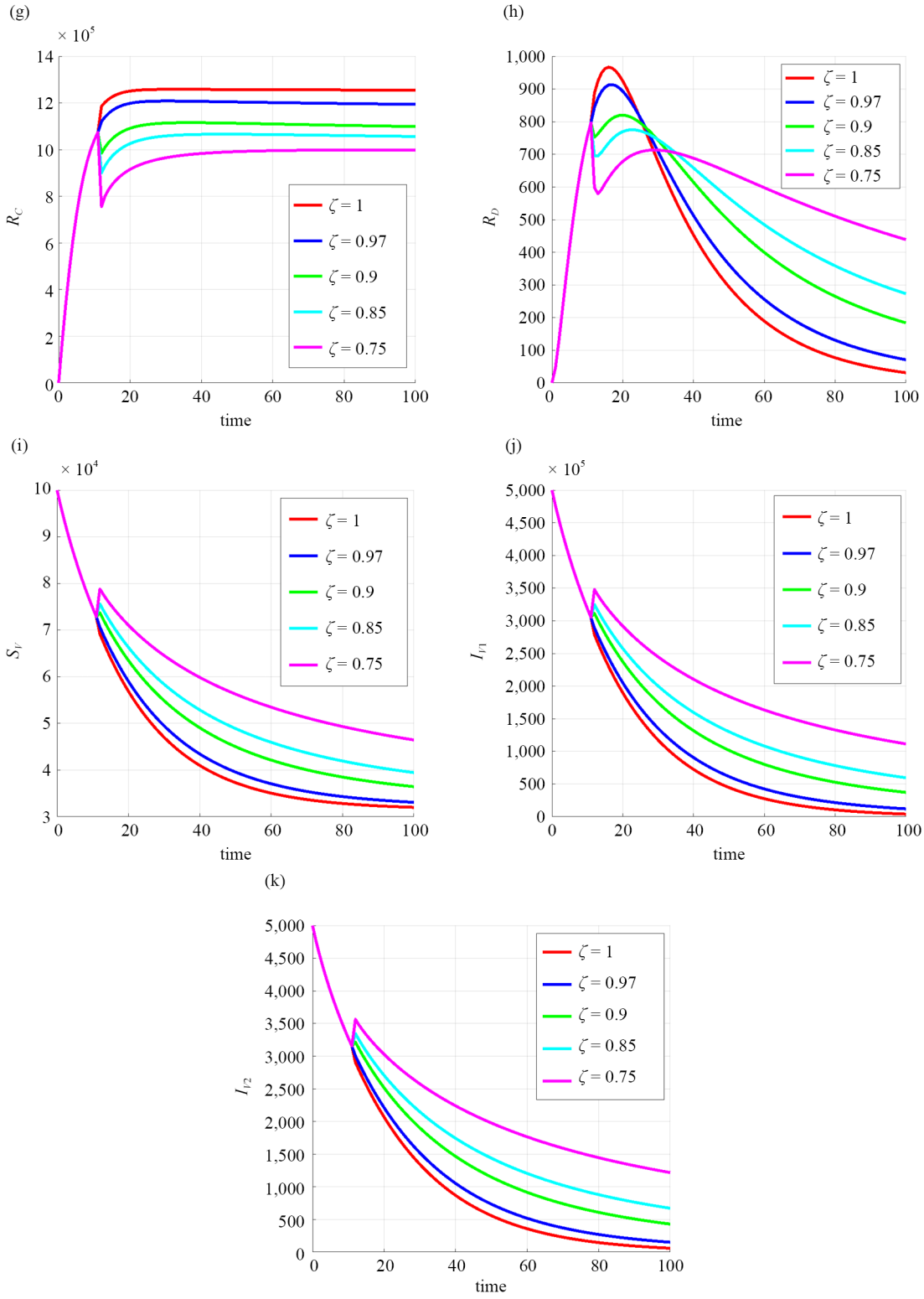

Figure 6. Simulation for second crossover model (14) and (12) with different ζ and $\zeta(t) = 0.96 - 0.0001(\sin(t/10))^2$

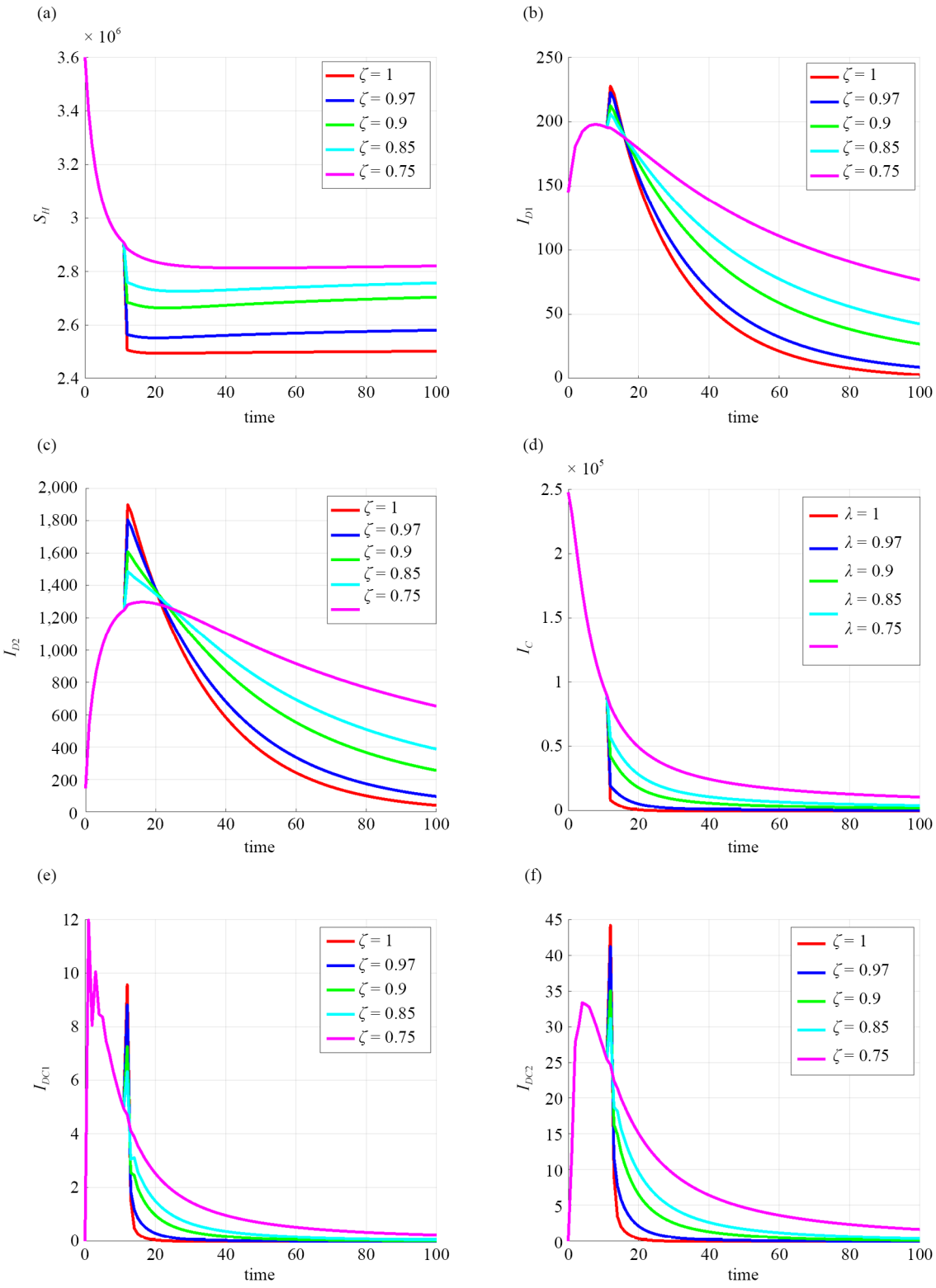
(a)
$\times 10^6$
S_H
time
$\zeta = 1$
$\zeta = 0.97$
$\zeta = 0.9$
$\zeta = 0.85$
$\zeta = 0.75$
(b)
I_{D1}
time
(c)
I_{D2}
time
(d)
$\times 10^5$
I_C
time
$\lambda = 1$
$\lambda = 0.97$
$\lambda = 0.9$
$\lambda = 0.85$
$\lambda = 0.75$
(e)
I_{DC1}
time
(f)
I_{DC2}
time

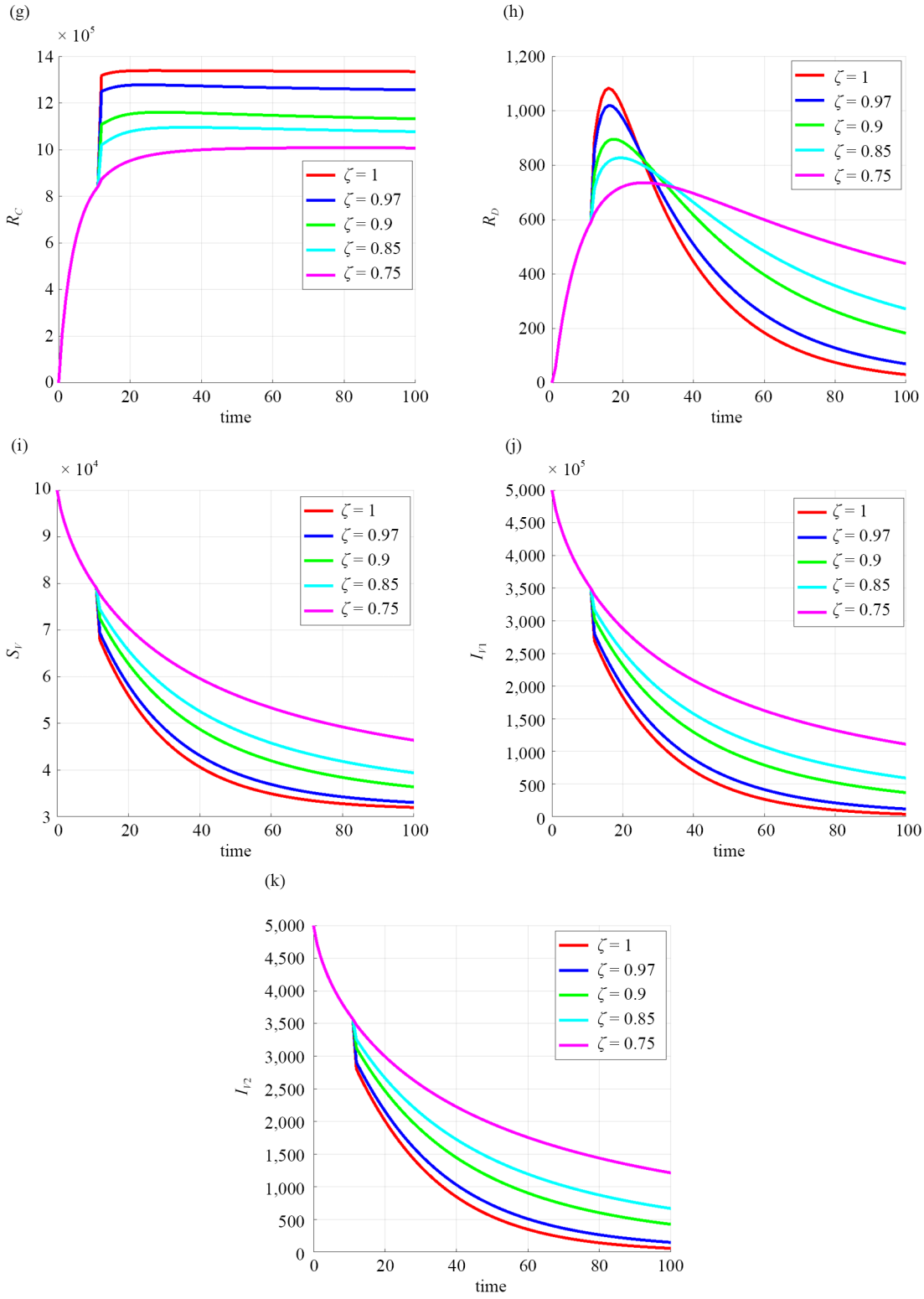

Figure 7. Simulation for second crossover model (14) and (12) with different order ζ and $\zeta(t) = 0.75 - 0.001t$

7.1 *Biological insights of constant fractional order ζ*

The inclusion of constant fractional order ζ introduces memory and hereditary effects into the model, enhancing its biological realism. The parameter $\zeta \in (0,\ 1]$ modulates how strongly the system remembers past states. Lower ζ values result in prolonged transitions between compartments, modeling biological phenomena such as delayed immune responses, prolonged latent periods, or gradual environmental adaptation.

• Higher ζ values simulate near-integer-order behavior, where transmission and recovery occur rapidly.

• Lower ζ values introduce inertia in the dynamics, ideal for capturing chronic or vector-borne diseases with complex temporal progression.

This modeling approach enables a better understanding of intervention timing and highlights critical phases where control measures may be most effective.

7.2 *Biological insights of variable-order fractional dynamics $\zeta(t)$*

Allowing the fractional order $\zeta(t)$ to vary with time further enhances the flexibility and biological fidelity of the model. This extension captures non-uniform temporal behaviors in disease transmission, which are common in real-world epidemiology due to environmental, seasonal, or behavioral factors.

• **Time-Dependent Adaptation:** Early in an outbreak, $\zeta(t) \approx 1$ reflects rapid transmission. As immunity builds or control measures take effect, $\zeta(t)$ decreases, representing slower, memory-dominated dynamics.

• **Environmental Seasonality:** Climate factors (e.g., temperature, humidity) that influence vector activity can be modeled through changes in $\zeta(t)$, enabling accurate predictions of seasonal outbreaks.

• **Immune and Pathogen Interference:** In co-circulation scenarios like dengue and COVID-19, $\zeta(t)$ captures adaptive immune responses or inter-pathogen effects such as cross-immunity.

• **Control Interventions:** Public health actions such as mass vaccination, awareness campaigns, or lockdowns can cause time-dependent shifts in disease dynamics, which are effectively represented by $\zeta(t)$.

• **Complex Disease Dynamics:** Variable-order models are ideal for multi-strain, multi-host infections with latent phases or varying infectivity, such as those seen in arboviruses or pandemics.

In summary, these simulations underscore the capability of fractional and variable-order models to reflect the intricate and evolving nature of infectious disease dynamics. By incorporating memory and environmental heterogeneity, these models offer a more nuanced and accurate framework for understanding, predicting, and ultimately controlling epidemic outbreaks.

7.3 *Discussion of numerical bifurcation results and crossover dynamics*

Figure 8 presents bifurcation diagrams illustrating the long-term behavior of the chronic infection class I_C as a function of the COVID-19 transmission rate β_c, under various fractional order and variable order with crossover model configurations. These results offer valuable insight into the qualitative dynamics of the system and how they change in response to transmission intensity.

The top-left panel shows the bifurcation structure for the classical model with constant order $\zeta(t) = 1$, which corresponds to standard integer-order dynamics. In this case, the system exhibits a forward (supercritical) transcritical bifurcation: the value of I_C remains near zero for small values of β_c, increases gradually as β_c crosses a critical threshold near $\beta_c \approx 0.7$, and subsequently decreases for larger values of β_c. This unimodal structure may result from saturation effects or competitive depletion of susceptible individuals as transmission increases.

The top-right and bottom panels correspond to crossover models incorporating variable fractional orders. Specifically, the top-right panel corresponds to the configuration where $\zeta = 0.8$ for $t \le t_1$, and $\zeta(t) = 0.98 - 0.0005t$ for $t > t_1$. The lower panel in turn represents the case $\zeta(t) = 0.98 - 0.0005t$ in the first interval and constant $\zeta = 0.8$ in the second. These crossover regimes introduce memory effects that vary across the simulation horizon, effectively capturing shifts in biological or environmental responsiveness.

In both crossover cases, the bifurcation diagrams display monotonic increases in I_C as β_c increases, differing markedly from the classical model. Notably, the variable-order model with strong memory effects throughout exhibits a more gradual

and persistent rise in infection prevalence, suggesting that memory kernels amplify endemicity and delay saturation. These dynamics underscore the biological realism added by fractional-order modeling, where systems retain past infection history, leading to sustained disease presence.

Overall, all three configurations confirm the occurrence of a forward transcritical bifurcation: the disease-free equilibrium is stable for small β_c, and an endemic equilibrium emerges smoothly as β_c crosses the threshold. No evidence of backward bifurcation, multistability, or oscillatory (Hopf) bifurcation is observed in any of the configurations. The primary impact of the fractional and crossover formulations lies in shifting the bifurcation threshold and reshaping the post-threshold dynamics.

These findings highlight the crucial role of memory effects in shaping epidemic transitions. The introduction of time-varying fractional orders alters the stability landscape, enhances infection persistence, and smoothens bifurcation transitions offering a more nuanced understanding of co-infection dynamics, particularly in the presence of long-term interactions such as immunity waning, environmental feedback, or treatment delays.

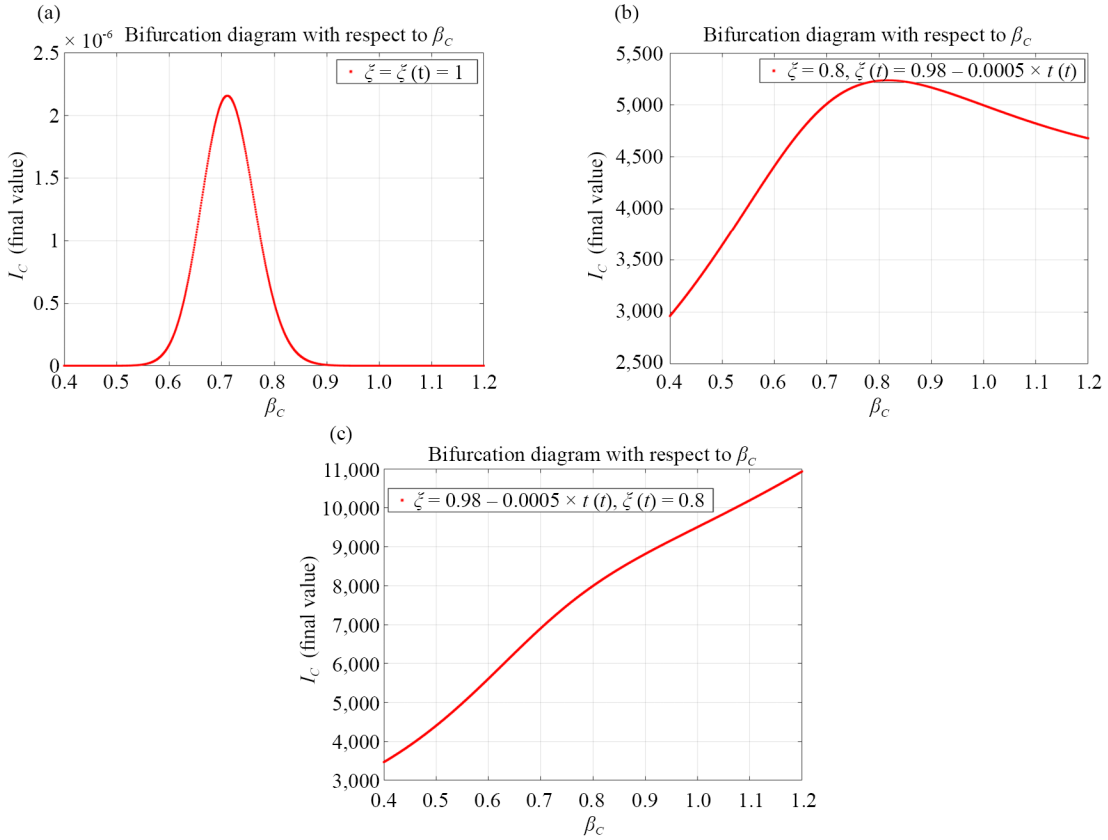

Figure 8. Bifurcation diagram for I_C with respect to β_C

8. Conclusions

This work presented a comprehensive discrete-time modeling framework for the co-circulation of two dengue virus strains and COVID-19 by integrating integer-order dynamics with advanced fractional and variable-order operators. We constructed four epidemiological models an integer-order baseline system, a fractional Caputo model, and two crossover models transitioning between constant-and variable-order operators to capture dynamic changes in memory effects, immunity, behavioral responses, and intervention phases. This multi-layered formulation offers a flexible and biologically realistic representation of real co-epidemic settings.

The analytical findings established key mathematical properties of the proposed systems, including positivity, boundedness, and the existence and uniqueness of solutions using Perov's fixed-point theorem in a generalized Banach space. The basic reproduction number was rigorously derived through the next-generation matrix method, and the local stability of the disease-free equilibrium was characterized. We further demonstrated that the systems undergo a forward (supercritical) transcritical bifurcation as the reproduction number crosses unity, confirming the transition between disease elimination and endemic persistence. The study also proved Ulam-Hyers stability and Lyapunov stability for the fractional and variable-order models, ensuring the robustness of the proposed formulations.

Many set of figures and numerical simulations illustrated the dynamic behavior of all model variants. These simulations emphasized how fractional memory, variable-order behavior, and crossover transitions significantly modify epidemic trajectories. The visual results clearly demonstrated differences in outbreak timing, peak magnitude, oscillation levels, and long-term persistence across the models. In particular, the crossover structures captured regime-shift phenomena that cannot be reproduced by classical or fixed-order models.

A comparison with existing works highlights several distinguishing features of the present study. While prior dengue-COVID-19 co-infection models have largely relied on integer-order or fixed-order differential operators, the proposed variable-order and crossover frameworks introduce a novel mechanism for modeling time-dependent memory effects and evolving transmission behavior. Additionally, previous studies rarely incorporated explicit co-infection compartments or transitions between epidemic-memory regimes. Therefore, the present work offers a more realistic and flexible modeling platform and extends the theoretical foundations of discrete fractional epidemiology beyond what is available in current literature.

Overall, this study provides a robust analytical and computational foundation for understanding the complex interactions governing dengue-COVID-19 co-epidemics. The proposed modeling approach not only advances theoretical epidemiology but also offers practical insights for public health planning, particularly in regions facing overlapping outbreaks. Future research may integrate optimal control strategies, real-data calibration, stochastic memory processes, and spatial dynamics to further enhance the applicability and predictive power of the presented models.

Future research may extend these models to incorporate spatial diffusion, multi-strain competition, stochastic perturbations, or optimal control frameworks, further enriching our understanding of complex epidemic systems in time-evolving environments.

Author contributions

The authors confirm their contribution to the paper as follows: Seham M. Al-Mekhlafi:Conceptualization, formal analysis, resources, software, supervision, writing original draft, methodology, validation, writing original draft, data collection. Ahmed Boudaoui and Noura Laksaci: Conceptualization, formal analysis, visualization, resources, writing original draft, Conceptualization, formal analysis, visualization. Thabet Abdeljawad: resources, supervision, data collection, methodology, validation, writing original draft, resources. Bahaaeldin Abdalla: Funding acquisition, resources, visualization. All authors reviewed the results and approved the final version of the manuscript.

Acknowledgement

The authors T. Abdeljawad and B. Abdalla would like to thank Prince Sultan University for paying the APC and for the support through the TAS research lab.

Conflicts of interest

The authors declare no conflicts of interest.

References

[1] UpToDate. *Dengue Virus Infection: Prevention and Treatment*. 2025. Available from: https://www.uptodate.com/contents/dengue-virus-infection-prevention-and-treatment/print [Accessed 26th March 2025].

[2] World Health Organization. *Dengue*. 2025. Available from: https://www.who.int/news-room/fact-sheets/detail/dengue-and-severe-dengue [Accessed 26th March 2025].

[3] Dupont-Rouzeyrol M, O'Connor O, Calvez E, Daurès M, John M, Grangeon JP, et al. Co-infection with Zika and Dengue Viruses in 2 Patients, New Caledonia, 2014. *Emerging Infectious Diseases*. 2015; 21(2): 381–382. Available from: https://doi.org/10.3201/eid2102.141553.

[4] Brady OJ, Gething PW, Bhatt S, Messina JP, Brownstein JS, Hoen AG, et al. Refining the global spatial limits of dengue virus transmission by evidence-based consensus. *PLOS Neglected Tropical Diseases*. 2012; 6(8): e1760. Available from: https://doi.org/10.1371/journal.pntd.0001760.

[5] Bhatt S, Gething PW, Brady OJ, Messina JP, Farlow AW, Moyes CL, et al. The global distribution and burden of dengue. *Nature*. 2013; 496(7446): 504–507. Available from: https://doi.org/10.1038/nature12060.

[6] World Health Organization. *Coronavirus Disease (COVID-19)*. 2025. Available from: https://www.who.int/health-topics/coronavirus [Accessed 26th March 2025].

[7] Katella K. *Omicron, Delta, Alpha, and More: What to Know About the Coronavirus Variants*. 2023. Available from: https://www.yalemedicine.org/news/covid-19-variants-of-concern-omicron [Accessed 26th April 2025].

[8] Omame A, Abbas M. The stability analysis of a co-circulation model for COVID-19, dengue, and zika with nonlinear incidence rates and vaccination strategies. *Healthcare Analytics*. 2023; 3: 100151. Available from: https://doi.org/10.1016/j.health.2023.100151.

[9] Ahmad W, Rafiq M, Butt AIK, Ahmad N, Ismaeel T, Malik S, et al. Analytical and numerical explorations of optimal control techniques for the bi-modal dynamics of Covid-19. *Nonlinear Dynamics*. 2024; 112(5): 3977–4006. Available from: https://doi.org/10.1007/s11071-023-09234-8.

[10] Butt AIK, Ahmad W, Rafiq M, Baleanu D. Numerical analysis of Atangana-Baleanu fractional model to understand the propagation of a novel corona virus pandemic. *Alexandria Engineering Journal*. 2022; 61(9): 7007–7027. Available from: https://doi.org/10.1016/j.aej.2021.12.042.

[11] Butt AIK, Ahmad W, Rafiq M, Ahmad N, Imran M. Optimally analyzed fractional Coronavirus model with Atangana-Baleanu derivative. *Results in Physics*. 2023; 53: 106929. Available from: https://doi.org/10.1016/j.rinp.2023.106929.

[12] Tchoumi SY, Rwezaura H, Tchuenche JM. Dynamic of a two-strain COVID-19 model with vaccination. *Results in Physics*. 2022; 39: 105777. Available from: https://doi.org/10.1016/j.rinp.2022.105777.

[13] Prapty CNBS, Rahmat R, Araf Y, Shounak SK, Noor-A-Afrin, Rahaman TI, et al. SARS-CoV-2 and dengue virus co-infection: Epidemiology, pathogenesis, diagnosis, treatment, and management. *Reviews in Medical Virology*. 2023; 33(1): e2340. Available from: https://doi.org/10.1002/rmv.2340.

[14] Tsheten T, Clements ACA, Gray DJ, Adhikary RK, Wangdi K. Clinical features and outcomes of COVID-19 and dengue co-infection: A systematic review. *BMC Infectious Diseases*. 2021; 21: 729. Available from: https://doi.org/10.1186/s12879-021-06409-9.

[15] Saddique A, Rana MS, Alam MM, Ikram A, Usman M, Salman M, et al. Emergence of co-infection of COVID-19 and dengue: A serious public health threat. *The Journal of Infection*. 2020; 81(6): 16–18. Available from: https://doi.org/10.1016/j.jinf.2020.08.009.

[16] Hanif A, Butt AIK. Atangana-Baleanu fractional dynamics of dengue fever with optimal control strategies. *AIMS Mathematics*. 2023; 8(7): 15499–15535. Available from: https://doi.org/10.3934/math.2023791.

[17] Abdeljawad T, Baleanu D. On fractional derivatives with exponential kernel and their discrete versions. *Reports on Mathematical Physics*. 2017; 80(1): 11–27. Available from: https://doi.org/10.1016/S0034-4877(17)30059-9.

[18] Wu GC, Baleanu D. Discrete fractional logistic map and its chaos. *Nonlinear Dynamics*. 2014; 75: 283–287. Available from: https://doi.org/10.1007/s11071-013-1065-7.

[19] Atici FM, Eloe PW. Discrete fractional calculus with the nabla operator. *Electronic Journal of Qualitative Theory of Differential Equations*. 2009; 2009(3): 1–12. Available from: https://doi.org/10.14232/ejqtde.2009.4.3.

[20] Goodrich C, Peterson AC. *Discrete Fractional Calculus*. Berlin/Heidelberg: Springer; 2015.

[21] Samko SG, Ross B. Integration and differentiation to a variable fractional order. *Integral Transforms and Special Functions*. 1993; 1(4): 277–300. Available from: https://doi.org/10.1080/10652469308819027.

[22] Shangerganesh L, Torres DFM. Modeling the dynamics of the Hepatitis B virus via a variable-order discrete system. *Chaos, Solitons and Fractals*. 2024; 184: 114987. Available from: https://doi.org/10.1016/j.chaos.2024.114987.

[23] Bushnaq S, Shafiullah, Sarwar M, Alrabaiah H. Existence theory and numerical simulations of variable order model of infectious disease. *Results in Applied Mathematics*. 2023; 19: 100395. Available from: https://doi.org/10.1016/j.rinam.2023.100395.

[24] Bushnaq S, Shah K, Tahir S, Ansari KJ, Sarwar M, Abdeljawad T. Computation of numerical solutions to variable order fractional differential equations by using non-orthogonal basis. *AIMS Mathematics*. 2022; 7(6): 10917–10938. Available from: https://doi.org/10.3934/math.2022610.

[25] Xu Y, He Z. Existence and uniqueness results for Cauchy problem of variable-order fractional differential equations. *Journal of Applied Mathematics and Computing*. 2013; 43: 295–306. Available from: https://doi.org/10.1007/s12190-013-0664-2.

[26] Al-Mekhlafi SM. A novel crossover variable order (deterministic stochastic) lung cancer and tumor-immune system interaction: Numerical simulations. *Progress in Fractional Differentiation and Applications*. 2025; 11(1): 73–86. Available from: https://doi.org/10.18576/pfda/110106.

[27] Al-Mekhlafi SM, Abou Hasan MM, Al-Ali HA, Mukandavire Z. A crossover optimal control framework for a time-delayed fractional-order diabetes model: Stability, bifurcation, and numerical analysis. *Mathematical Methods in the Applied Sciences*. 2025; 48(17): 15723–15741. Available from: https://doi.org/10.1002/mma.70046.

[28] Al-Mekhlafi SM. Numerical simulation of hybrid deterministic-stochastic PDE models for cancer tumor growth. *Research in Mathematics*. 2025; 12(1): 2567717. Available from: https://doi.org/10.1080/27684830.2025.2567717.

[29] Sen MD, Alonso-Quesada S, Ibeas A. On a discrete SEIR epidemic model with exposed infectivity, feedback vaccination and partial delayed re-susceptibility. *Mathematics*. 2021; 9: 520. Available from: https://doi.org/10.3390/math9050520.

[30] Sen MD, Alonso-Quesada S, Ibeas A, Nistal R. On a discrete SEIR epidemic model with two-doses delayed feedback vaccination control on the susceptible. *Vaccines*. 2021; 9: 398. Available from: https://doi.org/10.3390/vaccines9040398.

[31] Omae Y, Kakimoto Y, Sasaki M, Toyotani J, Hara K, Gon Y, et al. SIRVVD model-based verification of the effect of first and second doses of COVID-19/SARS-CoV-2 vaccination in Japan. *Mathematical Biosciences and Engineering*. 2021; 19: 1026–1040. Available from: https://doi.org/10.3934/mbe.2022047.

[32] Abdeljawad T. On Riemann and Caputo fractional differences. *Computers and Mathematics with Applications*. 2011; 62: 1602–1611. Available from: https://doi.org/10.1016/j.camwa.2011.03.036.

[33] Almatroud OA, Khennaoui A, Ouannas A, Grassi G, Al-sawalha MM, Gasri A. Dynamical analysis of a new chaotic fractional discrete-time system and its control. *Entropy*. 2020; 22: 1344. Available from: https://doi.org/10.3390/e22121344.

[34] Obiajulu EF, Omame A, Inyama SC, Diala UH, AlQahtani SA, Al-Rakhami MS, et al. Analysis of a non-integer order mathematical model for double strains of dengue and COVID-19 co-circulation using an efficient finite-difference method. *Scientific Reports*. 2023; 13: 17787. Available from: https://doi.org/10.1038/s41598-023-44825-w.

[35] van den Driessche P, Watmough J. Reproduction numbers and sub-threshold endemic equilibria for compartmental models of disease transmission. *Mathematical Biosciences*. 2002; 180(1): 29–48. Available from: https://doi.org/10.1016/S0025-5564(02)00108-6.

[36] Perov AI. On the Cauchy problem for a system of ordinary differential equations. *Problems and Methods of Solution of Differential Equations*. 1964; 2: 115–134.

[37] Akhmerov RR, Kamenskii MI, Potapov AS, Rodkina AE, Sadovskij BN. *Measures of Noncompactness and Condensing Operators*. Basel: Birkhäuser; 1992.

[38] City Population. *Brazil: Norte*. 2025. Available from: https://www.citypopulation.de/en/brazil/regiaonorte/admin/ [Accessed 10th August 2025].